Université de Montréal

Sur un système de deux oscillateurs FitzHugh-Nagumo couplés

par
Marcela Molinié

Département de mathématiques et statistique
Faculté des arts et des sciences

Mémoire présenté à la Faculté des études supérieures
en vue de l'obtention du grade de Maître ès sciences (M.Sc.)
en mathématiques

mai, 2012

Université de Montréal
Faculté des études supérieures

Ce mémoire intitulé:

Sur un système de deux oscillateurs FitzHugh-Nagumo couplés

présenté par:

Marcela Molinié

a été évalué par un jury composé des personnes suivantes:

Alain Vinet,   président-rapporteur
Jacques Bélair,   directeur de recherche
Christiane Rousseau,   membre du jury

Mémoire accepté le: . . . .

RÉSUMÉ

Ce mémoire consiste en l'étude du comportement dynamique de deux oscillateurs FitzHugh-Nagumo identiques couplés. Les paramètres considérés sont l'intensité du courant injecté et la force du couplage. Jusqu'à cinq solutions stationnaires, dont on analyse la stabilité asymptotique, peuvent co-exister selon les valeurs de ces paramètres. Une analyse de bifurcation, effectuée grâce à des méthodes tant analytiques que numériques, a permis de détecter différents types de bifurcations (point de selle, Hopf, doublement de période, hétéroclinique) émergeant surtout de la variation du paramètre de couplage. Une attention particulière est portée aux conséquences de la symétrie présente dans le système.

Mots clés: couplage, FitzHugh-Nagumo, bifurcation, non-linéaire, doublement de période, neurone.

ABSTRACT

We study the dynamical behaviour of a pair of identical, coupled FitzHugh-Nagumo oscillators. We determine the parameter values leading to the existence of up to five equilibrium solutions, and analyze the asymptotic stability of each one. A combination of analytical and numerical techniques is used to analyze the numerous bifurcations (saddle-node, Hopf, period-doubling, heteroclinic) occurring as parameters, most notably the coupling strength, are varied, attention being paid to the rôle played by symmetries in the system.

Keywords: coupling, FitzHugh-Nagumo, bifurcation, nonlinear, period doubling, neuron.

LISTE DES FIGURES

REMERCIEMENTS

Et finalement, le temps des remerciements arriva...

Il était une fois, une étudiante passionnée, mais fatiguée, tout court, qui décida de prendre un temps de réflexion avant de s'embarquer dans une maîtrise. Pensant s'éloigner peut être des études en mathématiques, elle entreprit ce qu'elle croyait être un dernier stage de recherche en ce domaine : mais il raviva sa flamme. Le plan de départ était de s'enfuir dans l'ouest jouer au rodéo sur les courants climatiques, mais ce projet de recherche, entrepris d'abord sans attentes, s'avéra plus captivant (et de longue haleine...) qu'elle ne l'avait espéré. Déjà embarquée dans cette aventure, je ne pouvais m'arrêter là. Le projet d'"hiver" devint projet de maîtrise.

Merci à mon directeur de recherche de m'avoir convaincue de rester. Dans nos entretiens, je me suis sentie d'abord intimidée, mais très tôt écoutée, appuyée, valorisée, inspirée. Mes réflexions avaient tout d'un coup un sens, un poids, un but. Dans cette lancée nous avons eu du mal à nous arrêter. J'ai eu du mal à accepter, qu'au fond, les questions n'arrêteraient jamais de se succéder.

Après la recherche vint la rédaction. Tous autour de moi, ma famille, mes amis, mon amoureux, peuvent en témoigner : ce fut douloureux. Merci de m'avoir soutenue, de m'avoir aidée à garder le moral, ces jours où l'indécision vis-à-vis le choix de chaque mot rendait l'écriture d'un paragraphe épique !

Merci Guillaume, mi corazón, de me prendre dans tes bras encore et toujours.

Gracias mamá, papá, pour votre sagesse, pour votre écoute, merci de m'avoir donné et d'avoir su nourrir en moi cette soif du savoir qui m'est si précieuse.

Merci aux professeurs qui m'ont enseigné et que j'ai côtoyés, votre empreinte je la porte, vous m'avez marquée.

Merci au département pour votre patience et votre bienveillance.

Merci et bonne lecture !

CHAPITRE 1

INTRODUCTION

1.1   La biologie mathématique : un domaine en croissance

L'essor à grande échelle de la modélisation mathématique en biologie est relativement récent. C'est surtout à partir des années 60 qu'on observe un développement plus marqué dans la complicité entre ces deux disciplines. Le rapprochement n'est pas nécessairement évident, entre les mathématiques, science qui se veut rigoureuse et exacte, et la biologie, d'une complexité quasi-insaisissable. Mais, au cours du XXe siècle, la biologie devient de plus en plus quantitative et l'évolution de la compréhension des systèmes biologiques motive l'utilisation de modèles.

La biologie mathématique englobe un large éventail de sous-domaines de la biologie, de l'écologie des populations à la physiologie, en passant par la biologie cellulaire. Parmi les modèles bio-mathématiques classiques, mentionnons les équations de Lotka-Volterra [29] décrivant l'interaction prédateur-proie. De nombreux modèles d'écologie des populations ont par la suite été dérivés pour tenir compte d'autres types d'interactions et de la coexistance d'espèces multiples dans un même écosystème. D'autres modèles traitaient des problèmes liés à la dispersion dans l'espace de populations animales et végétales, aux mouvements de micro-organismes, à la motricité de cellules dotées de flagelles, etc.

En épidémiologie, on crée des modèles pour mieux prédire l'évolution d'une maladie infectieuse dans une population, pouvoir ainsi agir plus efficacement face à une épidémie et répondre correctement aux questions comme : Quelle proportion de la population d'un pays devrait être vaccinée afin de freiner la propagation d'un virus de grippe ? Quelle fut la propagation spatiale de la peste en Europe lors de l'épidémie de 1347 à 1350 ?

La génétique compte aussi de nombreuses applications mathématiques au-

tant au niveau de la structure de l'ADN, que du séquençage du génome ou de la propagation d'un gène dans une population, dans ce dernier cas, nous pensons à la fameuse équation de Fisher-Kolmogorov [5]. Finalement, en biologie cellulaire et en physiologe, on tente de décrire la cinétique des réactions biochimiques, les échanges transmembranaires par diffusion ou canaux ioniques, la sécrétion pulsatile de certaines hormones comme l'insuline, l'adaptation de la rétine à la lumière, etc.

Il est indéniable que la liste est longue, et continuera à s'allonger. Mathématiques et biologie font bonne paire, s'enrichissant l'une l'autre, car il ne faut surtout pas négliger l'influence positive de la biologie sur les mathématiques. Ses problèmes stimulent la création de nouveaux modèles et motivent parfois la recherche de nouvelles façons de s'y prendre.

1.2   Modélisation mathématique et neurones

Le neurone est une cellule excitable, unité fonctionnelle de base du système nerveux. Sa caractéristique principale est sa capacité de générer un potentiel d'action, signal électrique qui se propage le long de l'axone, puis se transmet par les dendrites à des cellules avoisinantes. Le potentiel d'action se traduit par un changement soudain du potentiel trans-membranaire de la cellule.

C'est en 1952 que Hodgkin et Huxley [11] proposent le modèle de neurone le plus important, celui de l'axone géant de calmar. Ce modèle représente la membrane cellulaire du neurone comme un circuit électrique (voir le schéma à la figure 1.1) composé d'un condensateur en parallèle avec trois courants ioniques, celui du sodium (Na^+), celui du potassium (K^+) et un dernier englobant l'ensemble des autres courants ioniques dont celui du chlore (Cl^-). Ceci donne l'équation suivante :

$$I = C\frac{dv}{dt} + I_K + I_{Na} + I_L, \qquad \text{ou} \qquad C\frac{dv}{dt} = I - I_K - I_{Na} - I_L,$$

qui découle de la loi de Kirchhoff (loi des noeuds), le courant injecté total I

étant égal à la somme des courants ioniques et de $C\dfrac{dv}{dt}$, l'intensité du courant qui traverse le condensateur de capacité électrique C.
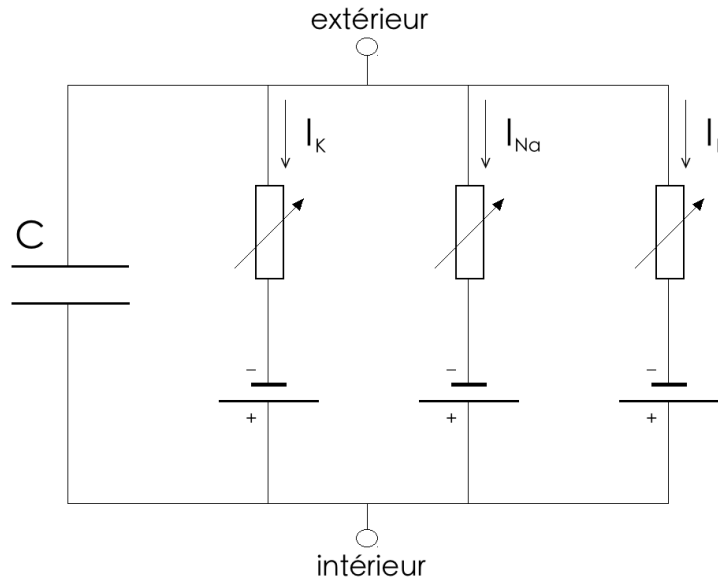
Figure 1.1 – Circuit électrique modélisant la membrane cellulaire du neurone, modèle de Hodgkin et Huxley : condensateur en parallèle avec trois courants ioniques.

Chacun des courants ioniques est proportionnel à la différence entre le potentiel membranaire et son potentiel de Nernst. Prenons l'exemple du potassium :

$$I_K = g_K(v - v_K).$$

Ici, le potentiel de Nernst est noté v_K. Celui-ci est unique pour chaque ion et est défini comme étant le potentiel pour lequel le gradient électrique et le gradient de concentration sont de forces égales et de sens opposés, engendrant un courant ionique nul. Le paramètre de proportionnalité est noté g_K, c'est la conductance de K^+. De la même façon, nous obtenons des expressions similaires pour les autres courants ioniques, d'où l'équation :

$$C\dfrac{dv}{dt} = I - g_K(v - v_K) - g_{Na}(v - v_{Na}) - g_L(v - v_L).$$

Les conductances ioniques, mis à part pour g_L, sont tout sauf constantes, dépendant notamment de l'état d'ouverture des canaux ioniques correspondants. Étant donné qu'on s'intéresse à l'état global de la population de canaux, on écrit la conductance comme le produit de la conductance maximale du type de canal en question, $\bar{g}$, et de la proportion de canaux ouverts, p :

$$g = \bar{g}p$$

Ici, nous considérons des canaux ioniques dits potentiel-dépendants. Le mécanisme d'ouverture et de fermeture des canaux consiste en un système de *portes*, de deux types, activation et inactivation, système contrôlé par des senseurs de potentiel. À titre d'exemple, supposons la présence d'une *porte* de chaque type. Le canal peut alors être fermé de deux façons, soit n'étant pas activé (*porte* d'activation non-ouverte), soit étant inactivé (*porte* d'inactivation qui bloque le passage aux ions). Dans cette optique, nous pouvons déterminer la proportion de canaux ouverts (ou probabilité qu'un canal soit ouvert) en fonction de la probabilité m qu'une *porte* d'activation soit ouverte et de la probabilité h qu'une *porte* d'inactivation soit ouverte. Supposant que les *portes* sont en séries, nous avons :

$$p = m^a h^b,$$

avec a et b les nombres de *portes* d'activation et d'inactivation par canal.

Grâce à la méthode de *voltage-clamp*, Hodgkin et Huxley ont pu déterminer les courants principaux entrant en jeux dans le courant transmembranaire de l'axone de calmar géant, leur conductance et les équations différentielles régissant les probalités d'ouverture des *portes* d'activation et d'inactivation. On désigne par m et h les probabilité d'ouverture des *portes* d'activation et d'inactivation des canaux de sodium et par n la probabilité d'ouverture des portes

d'activation des canaux de potassium. Le résultat est le modèle suivant :

$$\begin{cases} C\dfrac{dv}{dt} = -\bar{g}_K n^4(v - v_K) - \bar{g}_{Na} m^3 h(v - v_{Na}) - \bar{g}_L(v - v_L) + I \\ \dfrac{dm}{dt} = \alpha_m(v)(1 - m) - \beta_m(v)m \\ \dfrac{dn}{dt} = \alpha_n(v)(1 - n) - \beta_n(v)n \\ \dfrac{dh}{dt} = \alpha_h(v)(1 - h) - \beta_h(v)h \end{cases} \tag{1.1}$$

avec les fonctions α et β telles que proposées par Hodgkin et Huxley :

$$\begin{cases} \alpha_m(v) = 0.1\dfrac{25 - v}{\exp(\dfrac{25 - v}{10}) - 1}, & \beta_m = 4\exp(\dfrac{-v}{18}), \\ \alpha_h(v) = 0.07\exp(\dfrac{-v}{20}), & \beta_h = \dfrac{1}{\exp(\dfrac{30 - v}{10}) + 1}, \\ \alpha_n(v) = 0.01\dfrac{10 - v}{\exp(\dfrac{10 - v}{10}) - 1}, & \beta_n = 0.125\exp(\dfrac{-v}{80}), \end{cases} \tag{1.2}$$

et les constantes : $\bar{g}_{Na} = 120$, $\bar{g}_K = 36$, $\bar{g}_L = 0.3$. Ces équations sont pertinentes pour la température standard de la pieuvre de 6.3C. [11]

Une particularité importante de ce modèle est que certaines des variables sont rapides (v et m) et d'autres lentes (h et n). C'est sur la base de cette caractéristique qu'on peut s'appuyer pour élaborer un modèle plus simple tout en conservant les propriétés dynamiques importantes. En effet, si on s'intéresse au plan de phase v-n, on obtient une isocline verticale (en v) de forme cubique, et une isocline horizontale (en n) monotone croissante. Par conséquent, on peut représenter un neurone par le système de deux équations suivant :

$$\begin{cases} \dfrac{dv}{dt} = f(v) - w + I \\ \dfrac{dw}{dt} = av - bw + c \end{cases} \tag{1.3}$$
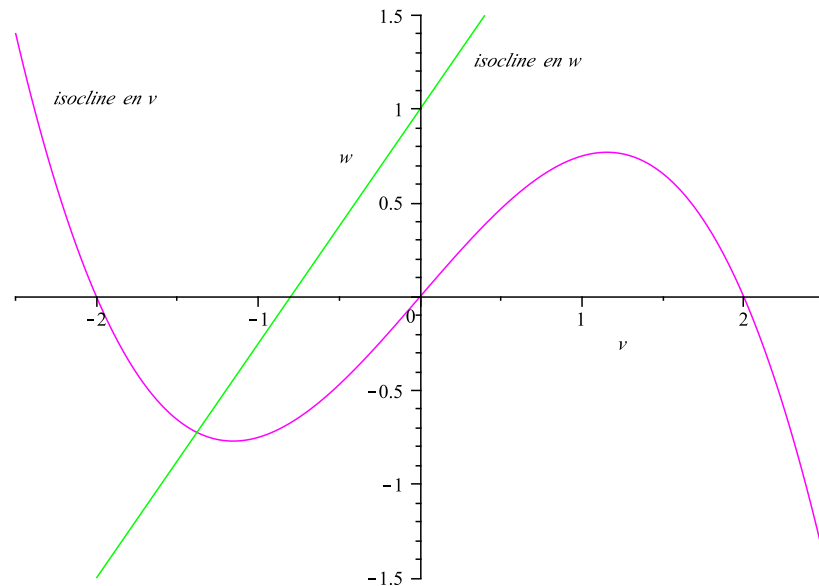
Figure 1.2 – Isoclines du système de FitzHugh-Nagumo (1.3), avec $f(v) = v - v^3/4$, $a = 5$ et $b = c = 4$.

avec $f(v)$ un polynôme cubique en forme de N inversé, et les constantes a, b positives. (voir figure 1.2) La variable v représente encore dans cette nouvelle version le potentiel de membrane, et w est une variable d'activation. Ce modèle proposé par FitzHugh en 1961 [6], est qualitativement équivalent à celui de Hodgkin et Huxley. Il conserve la capacité de générer des potentiels d'action, et une activité périodique de décharge de potentiels d'action (*firing*). Un potentiel d'action consiste en une dépolarisation du potentiel membranaire, ici représenté par v.

D'un autre point de vue, nous pouvons aussi voir ce modèle comme une autre représentation en circuit électrique, plus simple, de la membrane cellulaire. Ce modèle fut créé par Nagumo en 1962 [16] et consistait en un condensateur en parallèle avec une diode à effet tunnel d'une part, et d'autre part une résistance, un inducteur et une pile en série.

Un troisième et dernier modèle de neurone que nous évoquerons est celui de Hindmarsh-Rose (1984) [10], qui permettra d'introduire la section suivante et les motivations à l'origine de l'article qui constitue le corps de ce mémoire. Le

système d'équations est

$$\begin{cases} \dot{x} = y - x^3 + 3x^2 + I - z \\ \dot{y} = 1 - 5x^2 - y \\ \dot{z} = r(s(x - x_0) - z) \end{cases} \tag{1.4}$$

avec $x_0 = -\dfrac{1}{2}(1 + \sqrt{5})$ la coordonnée en x de la solution stationnaire stable du système :

$$\begin{cases} \dot{x} = y - x^3 + 3x^2 + I \\ \dot{y} = 1 - 5x^2 - y. \end{cases} \tag{1.5}$$

avec $I = 0$.

Ce modèle fut, à l'origine, élaboré pour reproduire la phénomènologie de modèles ioniques de haute dimension le plus simplement possible, notamment, pour recréer du *firing* rapide entrecoupé de longs intervalles, phénomène appelé *bursting*. L'idée était de remplacer le terme linéaire dans la deuxième équation du FHN par un terme quadratique. Après application d'une courte impulsion externe, le système adopte un état de *firing* rapide périodique, mais reste sur cette solution périodique. C'est enfin pour que le système puisse revenir à son état initial que la troisième variable z fut rajoutée. Pour des valeurs de r petites, celle-ci est une variable lente par rapport au sous-système 1.5, et son équation différentielle permet d'augmenter sa valeur quand le système est en *firing* rapide et ainsi, de diminuer le courant effectif $I - z$.

D'autres résultats intéressants furent éventuellement observés en faisant varier les paramètres r et s, le modèle étant capable de généner du *bursting*, régulier et chaotique.

1.3 Coeur, noeud sinusal et couplage

Le rythme cardiaque est contrôlé par la dépolarisation du noeud sinusal (SA), un groupe de cellules excitables situé au sommet de l'oreillette droite. Ces cellules ont une activité électrique oscillatoire qui, en se propageant à travers le myocarde, muscle cardiaque, produit les battements du coeur. Ainsi, le potentiel d'action qui voit le jour dans le noeud SA se propage à travers l'oreillette, qui se contracte, et converge vers le noeud atrio-ventriculaire (AV), dans la paroi inter-atriale, à la base de l'oreillette. Le potentiel d'action est ensuite communiqué aux cellules musculaires des deux ventricules à travers le faisceau de HIS, un réseau de cellules particulièrement conductrices appelées fibres de Purkinje. Cette propagation organisée d'un signal électrique se traduit finalement en contraction simultanée des parois ventriculaires.

Malheureusement, il arrive que des anomalies se produisent dans la séquence rythmique, provoquant des arythmies cardiaques. On pense par exemple à la tachycardie, accélération du rythme, qui diminue le débit, la fréquence de contraction étant trop élevée pour laisser le temps aux ventricules de se remplir entièrement. La fibrillation, de son côté, est une désorganisation de la propagation du signal, les cellules ne se contractent plus de façon coordonnée.

Le modèle Hodgkin-Huxley produit des potentiels d'action qui pourraient être similaires à ceux reçus par le noeud sinusal du système nerveux, surtout para-sympathique et a un comportement dynamique assez complexe, pouvant peut-être reproduire les anomalies citées ci-haut, devenant un bon candidat pour une modélisation des neurones liant système nerveux et coeur. Toutefois, si on veut modéliser un réseau d'oscillateurs, il est plus facile de faire un couplage avec un modèle plus simple. C'est ainsi que le modèle de Hindmarsh-Rose, par la diversité de ses solutions (*firing* rapide, *bursting*), devient un deuxième candidat intéressant.

Dans une tentative de simuler l'activité du noeud sinusal, Vinet et Jiang [28], voir [2] pour travail relié, ont proposé un réseau de quatre oscillateurs

Hindmarsh-Rose, avec un couplage agissant sur la variable lente z (voir 1.4). Leur méthode de recherche consistait essentiellement en une étude par simulations numériques. Il fut donc intéressant de procéder à une étude analytique détaillée, en commençant pas un système de deux oscillateurs Hindmarsh-Rose couplés. Les diagrammes de bifurcation obtenus à l'aide du logiciel XPPAUT générèrent la question à l'origine de ce mémoire : la complexité observée était-elle le fruit de la capacité du modèle Hindmarsh-Rose de produire du *bursting*, ou due au type de couplage utilisé, c'est-à-dire sur la variable lente, plutôt que sur une variable rapide ?

L'étape suivante fut de prendre un modèle encore plus simple, bidimensionnel, celui de FitzHugh-Nagumo étant le candidat naturel. Le couplage sur la variable de récupération w (voir équations 1.3), semblait au premier abord reproduire certaines des particularités du diagramme de bifurcation obtenu avec les oscillateurs Hindmarsh-Rose, attisant notre curiosité. À quel niveau de complexité pouvons nous nous attendre avec ce type de couplage ?

1.4 L'outil analytique, pour une compréhension globale

Dans l'article de Vinet et Jiang [28], [2], l'emphase fut mise sur les simulations numériques, dû à la complexité dynamique du modèle de Hindmarsh-Rose, accrue par un couplage de quatre de ces oscillateurs. Le défi que nous nous sommes posés était de faire une analyse de bifurcation détaillée d'un système de deux oscillateurs FitzHugh-Nagumo couplés, afin d'avoir une meilleure idée de l'effet du couplage sur la variable lente d'un modèle de cellules excitables.

L'outil idéal pour ce genre d'entreprise est bien entendu un programme de continuation et de bifurcation numérique. Le programme que nous avons choisi est celui de Bard Ermentrout, XPPAUT. Ce dernier contient le code pour AUTO, programme de continuation bien connu élaboré par Eusebius Doedel. Le va-et-vient facile et pratique entre les interfaces XPP et AUTO permet aussi de profiter des capacités de visualisation en parallèle des simulations, des plans de phase,

etc.

Le programme AUTO est construit autour de la méthode de continuation numérique. Cette dernière consiste à suivre une solution d'équilibre connue d'un système dynamique lorsque la valeur d'un paramètre varie. En effet, si la valeur du paramètre varie continûment, on s'attend à ce qu'il en soit de même pour la solution d'équilibre. On obtient alors une branche, famille de cette solution d'équilibre, par rapport au paramètre choisi, et on peut en détecter la stabilité ainsi que différents types de bifurcations. Les solutions qui peuvent être continuées sont stationnaires, périodiques, homocliniques, etc. L'ingéniosité des méthodes de continuation repose sur le fait que l'on peut considérer le paramètre comme une variable supplémentaire. À titre d'exemple, soit (x_0, p_0) tel que x_0 soit une solution d'équilibre du système $\dot{x} = f(x, p)$, avec $p = p_0$. On cherchera une nouvelle solution (x_1, p_1) telle que $f(x_1, p_1) = 0$. En général, la continuation consiste en une prédiction du nouveau point (x_1, p_1), à l'aide d'un vecteur de longueur s (pas de continuation), puis de sa correction, par convergence, en appliquant, par exemple, une méthode de Newton.

Deux autres outils logiciels ont été amplement utilisés, soient MATLAB et MAPLE. Et c'est armés de cet arsenal d'outils que nous avons pu affronter le défi de chercher une compréhension globale de la dynamique générée par le couplage symétrique sur la variable lente de deux oscillateurs FitzHugh-Nagumo.

CHAPITRE 2

BIFURCATION ANALYSIS OF A SYSTEM OF TWO COUPLED FITZHUGH-NAGUMO OSCILLATORS

Le contenu de ce chapitre est un manuscrit soumis au *SIAM Journal on Applied Mathematics*, dont les auteurs sont : Marcela Molinié et Jacques Bélair.

2.1 Introduction

The mathematical modeling of physiological rhythms has a long history, and was particularly formalized in the last century. From the pioneering work of van der Pol [27] to the groundbreaking studies of Hodgkin and Huxley [11], and then to the breathtaking conceptual advances of Winfree [30], numerous mathematical frameworks have been elaborated to try to get insight into the underlying fundamental physiological mechanisms.

One pervasive concern in all these studies is the question of *scales*, deciding the level of biological detail that is included in the mathematical description of the system under study. With the development of systems biology (in this century), the trend towards all inclusive representations has been exacerbated. But, to paraphrase Forsythe, the object of modeling is insight, not numbers, and we thus believe that there is much to be learned from analytic work on small networks [15].

Our motivation developed from an attempt to model the interaction between the neural activity and rhythmics of the sinus node with a network of Hindmarsh-Rose oscillators [2]. One of the questions that arose from the mainly numerical results concerned the determination of the real source of the dynamical particularities observed, namely to assess whether it was due to the spiking-bursting behaviour of the model (Hindmarsh-Rose), or to the symmetric coupling on the slow variables of the oscillators. Using FitzHugh-Nagumo [6] oscil-

lators is the natural, most direct simplification procedure that may nevertheless preserve the essential dynamical properties of the full system of equations.

This paper is organized as follows. After a brief review of the single oscillator, in Section 3 we introduce the system of two coupled oscillators; we consider its equilibrium solutions and investigate their stability, exploiting the symmetries in the system. In section 4 we use a combination of analytical and numerical (continuation) techniques to investigate the successive bifurcations occurring after the equilibria have become unstable. We find that numerous period-doubling sequences occur, and homoclinic bifurcations as well.

2.2 Single FitzHugh-Nagumo Oscillator

We briefly review the analysis of the behaviour of the FitzHugh-Nagumo equations

$$
\begin{cases}
\dot{v} = v - \frac{v^3}{3} - w + is \\
\dot{w} = \delta(v + a - bw)
\end{cases}
\tag{2.1}
$$

in which the parameters take the respective values $\delta = 0.08$, a=0.7 and b=0.8, and the variables are traditionally interpreted as an electrical potential v, which is a fast variable, and w represents the inactivation of sodium channels (slow variable). The bifurcation parameter of choice is the stimulation current is which we take to be constant and real.

2.2.1 Equilibrium points

We first determine the equilibrium points, or stationary solutions, of equations (2.1). Any and all such points (v_0, w_0) must satisfy the equations

$$
\begin{cases}
p(v_0) = 0 \\
w_0 = \frac{v_0 + a}{b}
\end{cases}
\tag{2.2}
$$

with $p(v) := -\frac{v^3}{3} + (1 - \frac{1}{b})v + (is - \frac{a}{b})$. This cubic polynomial can have up to three real roots, depending on the value of b. Indeed, since

$$p'(v) = -v^2 + (1 - \frac{1}{b}) \tag{2.3}$$

if $0 < b \leqslant 1$, $p'(v) < 0$, then p is decreasing for all real values of v. The solution of equations (2.2) is then unique. If either $b < 0$ or $b > 1$, then this derivative has two real roots $v_{1,2} = \pm\sqrt{1 - \frac{1}{b}}$, and again between those values, p decreases. Whatever the value of b, the polynomial $p(v)$ can indeed have up to 3 real roots.

To simplify the following analysis, we fix b at the value 0.8, in which cases, $p(v)$ has only one real root, thus eliminating the possibility of homoclinic bifurcations in equations (2.1).

2.2.2 Linear Stability

Let v_0 denote the unique real root of $p(v)$ and $w_0 = \frac{v_0 + a}{b}$, so that the equilibrium point of system (2.1) is (v_0, w_0). According to the first equation of (2.2), we can express the parameter is as a function of v_0 :

$$is(v_0) = \frac{v_0^3}{3} + (\frac{1}{b} - 1)v_0 + \frac{a}{b}. \tag{2.4}$$

Since this relation is one-to-one and onto in the parameter range of a and b under investigation, we can choose to represent the bifurcation diagram of the equilibrium points as a function of either its v-coordinate, v_0, or the parameter is. We then project the result as a curve $is = is(v_0)$.

By linearizing the system (2.1) around the steady state (v_0, w_0), we get the Jacobian matrix

$$J_1 := \begin{pmatrix} 1 - v_0^2 & -1 \\ \delta & -b\delta \end{pmatrix} \tag{2.5}$$

with eigenvalues

$$\lambda_{1,2} = \frac{-(b\delta + v_0^2 - 1) \pm \sqrt{\Delta}}{2}, \tag{2.6}$$

where $\Delta := (b\delta + v_0^2 - 1)^2 - 4\delta(1 - b(1 - v_0^2))$.

The sign of the discriminant Δ determines whether the eigenvalues are purely real or complex conjugates. By introducing $u := v_0^2$, in the definition of Δ, we can write

$$\Delta(u) = u^2 - 2(b\delta + 1)u + (b\delta + 1)^2 - 4\delta$$

and its zeros (solutions of $\Delta(u) = 0$) as

$$u_{1,2} = (b\delta + 1) \pm 2\sqrt{\delta}. \tag{2.7}$$

Since $\Delta(u)$ is a second degree polynomial with positive first coefficient, then $\Delta < 0$ and the eigenvalues of J_1 are complex conjugates if and only if $v_0^2 \in]u_1, u_2[$. We thus obtain

$$\begin{cases} \lambda_{1,2} \in \mathbb{C}, & \text{if } v_0 \in I, \\ \lambda_{1,2} \in \mathbb{R}, & \text{if } v_0 \notin I, \end{cases} \tag{2.8}$$

with I the union of two intervals defined by $I :=] - \sqrt{u_2}, -\sqrt{u_1}[\cup]\sqrt{u_1}, \sqrt{u_2}[$.

When $\Delta < 0$, the sign of the real part of the eigenvalues is the same as that of $-(b\delta + v_0^2 - 1)$, and thus,

$$-(b\delta + v_0^2 - 1) < 0 \Leftrightarrow v_0^2 > 1 - b\delta$$
$$\Leftrightarrow v_0 \notin H, \tag{2.9}$$

where H is the interval $H := [-h, h]$, with $h := \sqrt{1 - b\delta}$. Then we have $\Delta < 0$,

when v_0 lies outside the interval H.

Since $\pm h \in I$, there are two possible Hopf bifurcations at $v_0 = \pm h$, and the sign of the real parts of the eigenvalue λ_i is given by

$$\begin{cases} Re((\lambda_i)) < 0, \text{ if } v_0 \in I \smallsetminus H =]-\sqrt{u_2}, -h[\cup]h, \sqrt{u_2}[, \\ Re((\lambda_i)) \geq 0, \text{ if } v_0 \in I \cap H = [-h, -\sqrt{u_1}[\cup]\sqrt{u_1}, h]. \end{cases}$$

If $\Delta > 0$ and both eigenvalues are real, the sign of these eigenvalues will be the same as that of $-(b\delta + v_0^2 - 1)$ since $\sqrt{\Delta} < |b\delta + v_0^2 - 1|$ for all real values of v_0. Indeed,

$$\Delta > (b\delta + v_0^2 - 1)^2 \Leftrightarrow v_0^2 < 1 - \frac{1}{b}. \tag{2.10}$$

Thus, when $\delta > 0$, we have :

$$\begin{cases} \lambda_i < 0, \text{ if } v_0 \notin [-\sqrt{u_2}, \sqrt{u_2}], \\ \lambda_i > 0, \text{ if } v_0 \in [\sqrt{u_1}, \sqrt{u_1}]. \end{cases}$$

where u_1 and u_2 are defined in equations (2.7).

The results of this Section are summarized in figure 2.1, where we represent the v-coordinate of the unique equilibrium point as function of the continuation program parameter *is*. The color of the line illustrates the nature of its eigenvalues. There are two stability changes happening at the Hopf bifurcation points $v = \pm h$. The equilibrium point is a node for most of the values of the parameter, but there are two intervals around the bifurcations where this equilibrium point is a focus, leading to the creation of a periodic solution.

To determine a complete bifurcation diagram, we have used the continuation program XPPAUT to produce figure 2.2 in which we see the predicted Hopf bifurcations, as well as the ensuing limit cycles. We also observe a change of stability at two limit points : as we zoom on the Hopf bifurcations, we determine
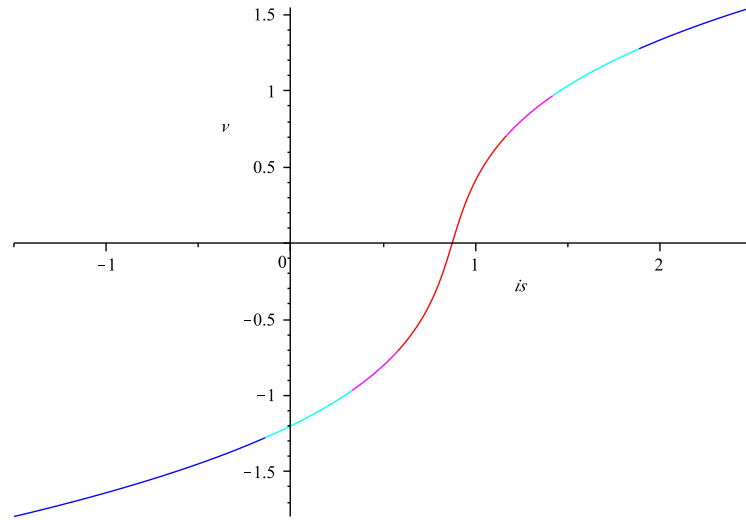
Figure 2.1 – Stability Portrait of equilibrium (v_0, w_0). Red :repelling node, magenta :repelling focus, light blue : attracting focus, and blue : attracting node.

both of them to be subcritical, leading to unstable limit cycles existing when the equilibrium point is stable. This can be analytically confirmed by the following calculations.

Putting system (2.1) in a real Jordan form with its equilibrium point at the origin in a neighbourhood of the Hopf bifurcation points yields

$$\begin{cases} \dot{x} = \mu x - \omega y - \frac{v_0(1-v_0^2+b\delta)}{\sqrt{-\Delta}}y^2 - \frac{1-v_0^2+b\delta}{3\sqrt{-\Delta}}y^3 \\ \dot{y} = \omega x + \mu y - v_0 y^2 - \frac{1}{3}y^3 \end{cases} \tag{2.11}$$

where the bifurcation parameter considered is v_0 (*is* has been replaced by its expression as a function of v_0). The Lyapunov number at the Hopf bifurcations can be calculated to be $\sigma \approx 9.89 > 0$ (eq. 3.4.11 in [8]), leading to subcritical Hopf bifurcations at both values of Δ for which $\mu = 0$.

As a function of *is*, there are two small regions around the Hopf bifurcations (figure 2.2) where a stable equilibrium point and two periodic solutions coexist, one unstable and the other, with a bigger amplitude, stable. For values of *is* bet-
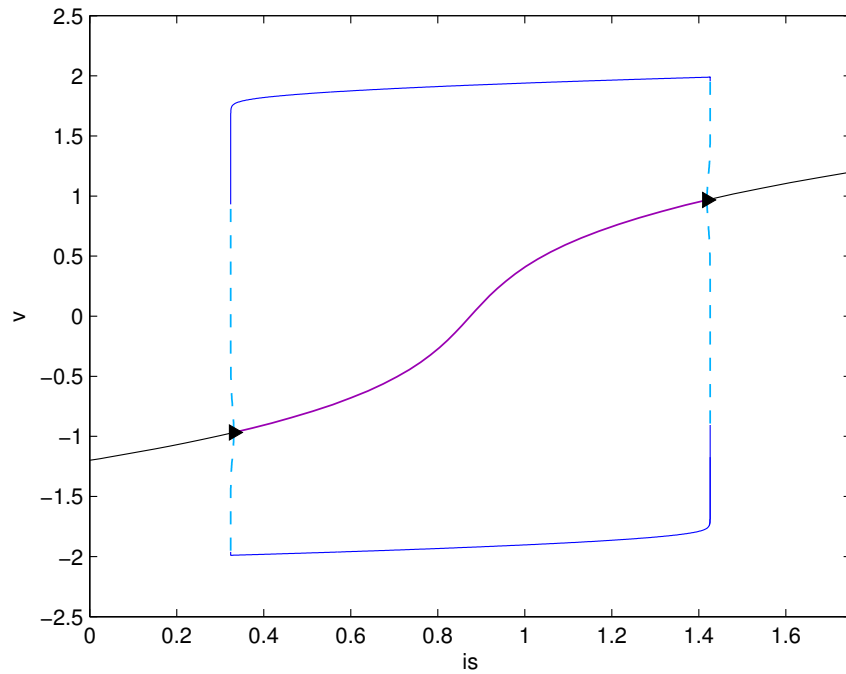
(a) Bifurcation diagram for equations 2.1, v in function of the parameter is
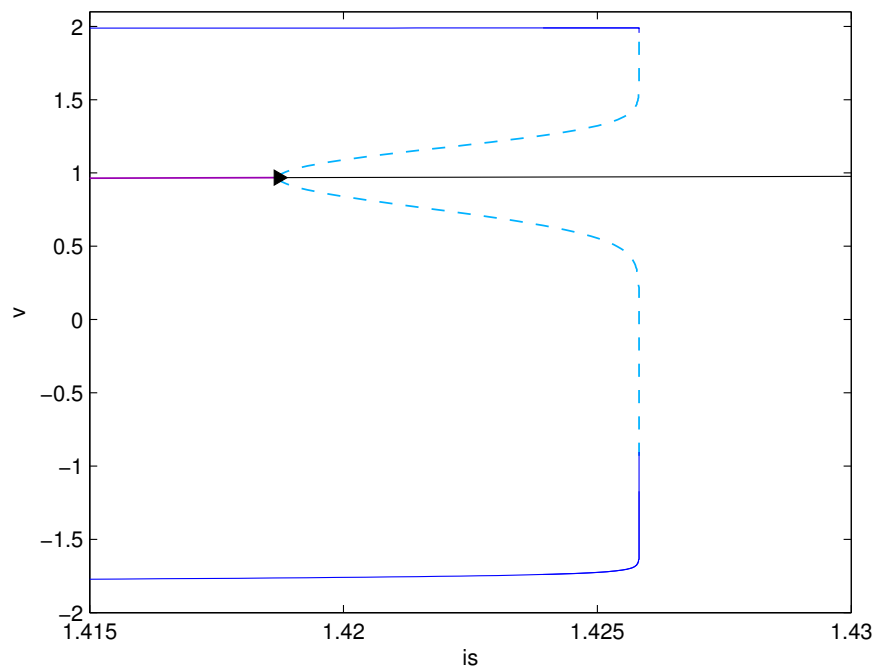
(b) Zoom of the diagram in (a) on the Hopf bifurcation on the right ($1.415 \leqslant is \leqslant$ 1.43). We can clearly see it to be subcritical. Notice the saddle-node bifurcations of the periodic orbit.

Figure 2.2 – Black and purple lines represent steady states, respectively stable and unstable. Dark blue and dashed light blue represent periodic solutions, stable and unstable respectively.

ween those intervals, there is only one stable limit cycle, and the steady state is unstable. For values of *is* outside the interval of existence of at least one periodic solution, a quiescent behavior is observed, as all trajectories are attracted to the equilibrium point.

2.3   Two Coupled Oscillators

We can now turn to the system of two identical Fitzhugh-Nagumo oscillators submitted to the same external stimulus *is*, and symmetrically coupled, namely

$$
\begin{cases}
\dot{v}_1 = v_1 - \frac{v_1^3}{3} - w_1 + is \\
\dot{w}_1 = \delta(v_1 + a - bw_1) + \varepsilon(v_2 - v_1) \\
\dot{v}_2 = v_2 - \frac{v_2^3}{3} - w_2 + is \\
\dot{w}_2 = \delta(v_2 + a - bw_2) + \varepsilon(v_1 - v_2).
\end{cases}
\tag{2.12}
$$

As discussed in the Introduction, the coupling term is applied on the slow variables, not the more common electrical coupling via the flow of ions through the gap junctions. The difference between the fast variables v_1 and v_2 acts symmetrically on the slow variables w_1 and w_2, with ε as the parameter measuring the intensity of the coupling. We get anti-diffusive coupling for $\varepsilon > 0$, that is if $v_1 > v_2$, there is a negative effect on v_2 and a positive one on v_1 ; for $\varepsilon < 0$, the coupling is diffusive. We will see that the set of dynamical behaviors produced by the system (2.12) is particularly rich for an interval of values of the coupling parameter around zero.

2.3.1 Equilibrium Points

We begin by looking for equilibrium solutions $(v_1^0, w_1^0, v_2^0, w_2^0)$ of system (2.12).
For $\varepsilon \neq 0$, these have to satisfy the set of equations :

$$\begin{cases} v_i = q(v_j) \\ w_i = \frac{v_i + a}{b} + \frac{\varepsilon}{b\delta}(v_j - v_i) \end{cases} \tag{2.13}$$

with $i, j = 1, 2$, $i \neq j$, and $q(v) := \frac{b\delta}{\varepsilon}\{-\frac{v^3}{3} + v(1 - \frac{1}{b}(1 - \frac{\varepsilon}{\delta})) + (is - \frac{a}{b})\} = \frac{b\delta}{\epsilon}p(v) + v$,
where $p(v)$ is defined just after equations (2.2) . Due to the symmetry of the cou-
pling, equations (2.12) describe two uncoupled identical oscillators when $v_1 = v_2$.
In which case, from equations (2.13) we get $w_1 = w_2$, and since $v = q(v) \Leftrightarrow p(v) = 0$ and p has a unique root, only one equilibrium can exist for equations (2.12),
and it is given by $P_0 := (v_0, w_0, v_0, w_0)$, with (v_0, w_0) the equilibrium point of the
uncoupled system (2.1), which is therefore the unique symmetric steady state
of system (2.12). Here, P_0 depends only on the parameter is, and exists for all
values of is and ε.

We observe, using the continuation software XPPAUT, a parameter range in
is for which two other pairs of equilibrium points, depending on both parame-
ters is and ε, do exist. Two new branches of equilibria emerge from P_0 at a value
close to $\varepsilon = 0.008$, and undergo a fold for $\varepsilon \gtrsim 0.009604$ (see figure 2.3). The first
value, as we will see later, corresponds to the apparition of branch points on the
branch of P_0 and can be found by a linear analysis of the system by looking at the
eigenvalues of the linearized system near P_0. The second one, observed nume-
rically, has been found by a series of continuations of the equilibrium point for
different values of ε in the interval $[0.0081, 0.1]$. Since there has been no theore-
tical analysis on the two other branches of equilibrium points, we have no exact
expression for the value of ε at which the folds appear. In figure 2.3c, we only
show the folds near the right hand side branch point, but there is a similar fold
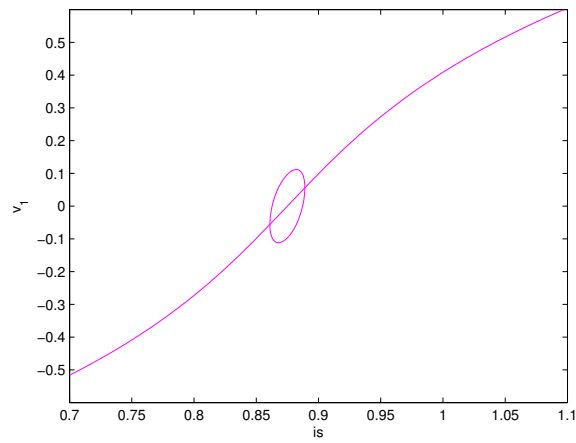
(a) Locus of stationary solutions of system (2.12) displaying v_1 as a function of *is* for $\varepsilon = 0.0081$.
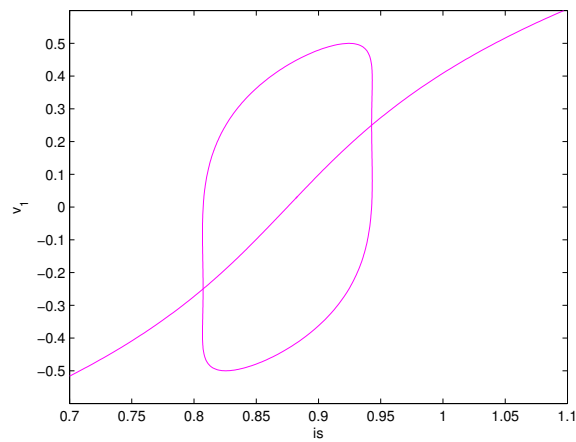
(b) Locus of stationary solutions of system (2.12) displaying v_1 as a function of *is* for $\varepsilon = 0.01$
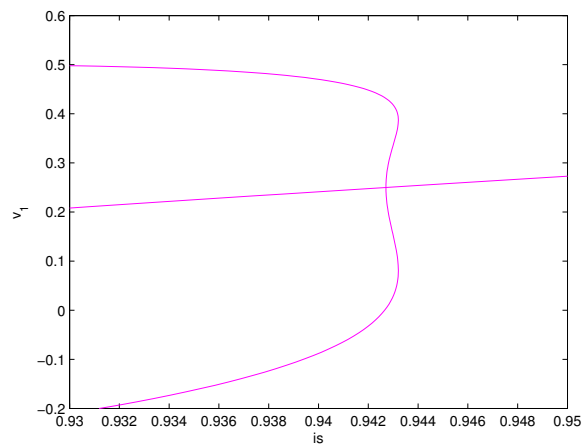
(c) Zoom on the right hand side branch point of figure 2.3b

Figure 2.3 – Creation of the new stationary solution branches. Near $\varepsilon = 0.008$.

near the other branch point.

The existence of at most five steady states of the system (2.12) can be determined from a geometrical point of view. Indeed, solving equations (2.13) is equivalent to finding the intersection points of the curves $C_1 := \{(v_1, v_2) : q(v_1) = v_2\}$ and $C_2 := \{(v_1, v_2) : q(v_2) = v_1\}$, which are symmetric with respect to the line $v_2 = v_1$, as illustrated in figure 2.4. From the degree of the polynomial $q(q(v))$ alone, we know there can be up to nine solutions. However, in order for this polynomial to have more than five solutions, the symmetric curves would have to intersect along the line $v_2 = v_1$ more than once which is clearly, from a geometrical point of view, impossible. Thus, there cannot be more than five intersection points.

2.3.2 Linear Stability of P_0

The stability of the equilibrium point P_0 is closely related to the stability properties of the equilibrium of the single oscillator. In fact, only two of the four eigenvalues of the Jacobian matrix of the linearization at the equilibrium P_0 depend on the coupling parameter ε . This is a general result, not restricted to the FitzHugh-Nagumo equations, but rather due to the symmetry in the coupling. Indeed, consider the system

$$
\begin{cases}
\begin{pmatrix} \dot{X}_1 \\ \dot{Y}_1 \end{pmatrix} = F(X_1, Y_1) + \begin{pmatrix} 0 \\ \varepsilon(X_2 - X_1) \end{pmatrix} \\
\begin{pmatrix} \dot{X}_2 \\ \dot{Y}_2 \end{pmatrix} = F(X_2, Y_2) + \begin{pmatrix} 0 \\ \varepsilon(X_1 - X_2) \end{pmatrix}.
\end{cases}
\tag{2.14}
$$

(a) *is* = 0.44   (b) *is* = 0.54   (c) *is* = 0.74
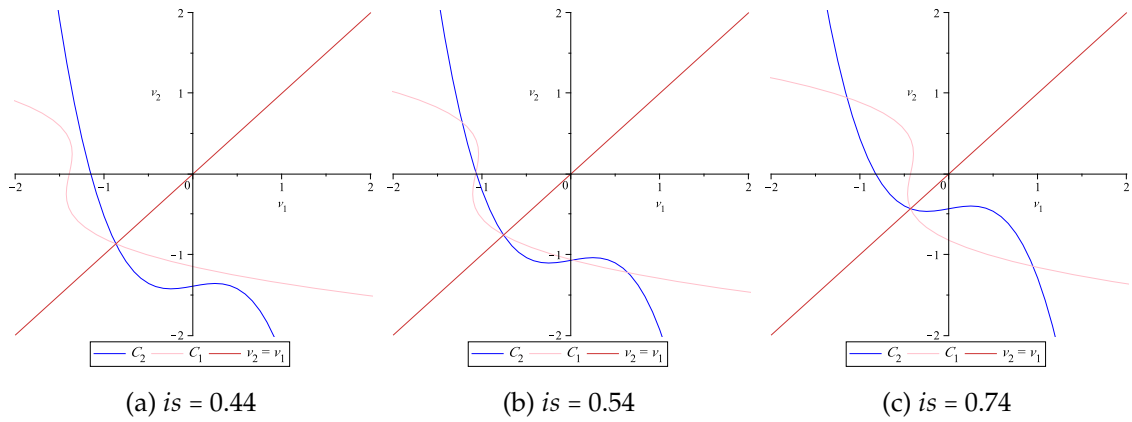
Figure 2.4 – The curves C_1 and C_2 (defined in the text) for $\varepsilon = 0.02$ and different values of *is*.

where $F(X_i, Y_i) = (f(X_i, Y_i) \; g(X_i, Y_i))^T$ is a vector-valued function such that the system

$$\begin{cases} \dot{X}_1 = f(X_1, Y_1) \\ \dot{X}_2 = g(X_2, Y_2) \end{cases} \tag{2.15}$$

possesses a unique stationary solution (X_0, Y_0). It is easy to see that this equilibrium state of the two-dimensional system can be used to construct the 4-dimensional stationary solution (X_0, Y_0, X_0, Y_0) of equations (2.14). By linearizing the latter system around this equilibrium, we obtain the Jacobian matrix

$$J_2 = \begin{pmatrix} J_1 - B_\varepsilon & B_\varepsilon \\ B_\varepsilon & J_1 - B_\varepsilon \end{pmatrix}$$

where $J_1 := Df(X_0, Y_0)$, and $B_\varepsilon := \begin{pmatrix} 0 & 0 \\ \varepsilon & 0 \end{pmatrix}$. By an appropriate change of coordinates, the matrix J_2 can be put in the following block diagonal form :

$$\begin{pmatrix} J_1 & 0 \\ 0 & J_1 - 2B_\varepsilon \end{pmatrix}.$$

In this form, it becomes obvious that two of the eigenvalues of J_2 are the eigenvalues of the matrix J_1 defined in equation (2.5), that is, the eigenvalues corresponding to the linearization of the uncoupled system around its equilibrium point (X_0, Y_0), and that the remaining two eigenvalues of J_2 are the eigenvalues of the matrix $J_1 - 2B_\varepsilon$.

To set the notation for the subsequent analysis, in which we systematically determine the distribution in parameter space of the four eigenvalues of the linearized system, we denote by λ_1 and λ_2 the eigenvalues of J_1 and let λ_3, λ_4 be the eigenvalues of the complementary matrix

$$J_1 - 2B_\varepsilon = \begin{pmatrix} 1 - v_0^2 & -1 \\ \delta - 2\varepsilon & -b\delta \end{pmatrix}.$$

2.3.2.1 Distribution of λ_1 and λ_2

These eigenvalues, λ_1 and λ_2, have the same values as the eigenvalues of the linearized single oscillator, and they depend only on the stimulation current parameter is, or on the value of v_0 (and not on the coupling strength ε, obviously). The region of stability of this equilibrium in the two-dimensional space were computed to be :

$$\text{if } v_0 \in I \Rightarrow \lambda_{1,2} \in \mathbb{C}, \begin{cases} \text{and if } v_0 \notin H \Rightarrow Re(\lambda_{1,2}) < 0 \\ \text{and if } v_0 \in H \Rightarrow Re(\lambda_{1,2}) > 0 \end{cases}$$

$$\text{if } v_0 \notin I \Rightarrow \lambda_{1,2} \in \mathbb{R}, \begin{cases} \text{and if } v_0 \notin H \Rightarrow \lambda_1 \text{et } \lambda_2 < 0 \\ \text{and if } v_0 \in H \Rightarrow \lambda_1 \text{et } \lambda_2 > 0 \end{cases}$$

with I and H were defined just after equations (2.8) and (2.9), respectively.

2.3.2.2 Distribution of λ_3 and λ_4

The eigenvalues of the matrix $J_1 - 2B_\varepsilon$ satisfy the characteristic equation

$$\lambda^2 + \lambda(b\delta + v_0^2 - 1) + \delta(1 - b(1 - v_0^2)) - 2\varepsilon = 0,$$

so that

$$\lambda_{3,4} := \frac{-(b\delta + v_0^2 - 1) \pm \sqrt{\Delta'}}{2} \tag{2.16}$$

where $\Delta' := (b\delta + v_0^2 - 1)^2 - 4[\delta(1 - b(1 - v_0^2)) - 2\varepsilon] = \Delta + 8\varepsilon$.

By a calculation similar to that of Section 2.2 above, by introducing the auxiliary variable $r := v_0^2$, we obtain that if $v_0^2 \in \,]r_1, r_2[$, where

$$r_{1,2} = (b\delta + 1) \pm 2\sqrt{\delta - 2\varepsilon}, \tag{2.17}$$

then $\Delta' < 0$ and the eigenvalues $\lambda_{3,4}$ of J_2 are complex conjugates.

However, in this case, these values $r_{1,2}$ clearly depend on ε. If we want instead to express the relation between ε and v_0 in terms of v_0 only, we can rearrange the inequality corresponding to $v_0^2 \in \,]r_1, r_2[$ as follows :

$$r_1 < v_0^2 < r_2$$

$$\Leftrightarrow -\sqrt{\delta - 2\varepsilon} < \frac{v_0^2 - (b\delta + 1)}{2} < \sqrt{\delta - 2\varepsilon}$$

$$\Leftrightarrow \delta - 2\varepsilon > \left(\frac{v_0^2 - (b\delta + 1)}{2}\right)^2$$

$$\Leftrightarrow \varepsilon < \frac{\delta - \left(\frac{v_0^2 - (b\delta + 1)}{2}\right)^2}{2} =: \varepsilon_c(v_0) \tag{2.18}$$

This function $\varepsilon_c(v_0)$ is a quartic polynomial in v_0, symmetric about $v_0 = 0$, which has two maxima. Therefore, as ε increases, the interval of values of v_0 where the eigenvalues $\lambda_{3,4}$ are complex conjugate goes from being one single continuous interval to becoming the union of two symmetric intervals, before finally disap-

pearing at the maxima, where $\varepsilon = \varepsilon_c(\pm\sqrt{b\delta + 1}) = \frac{\delta}{2} = 0.04$. When $\varepsilon = 0$, we have $u_{1,2} = r_{1,2}$.

Note that according to equations (2.6) and (2.16), the real parts of the two couples of eigenvalues of P_0 are equal, $Re(\lambda_{1,2}) = Re(\lambda_{3,4})$, hence the sign of the real parts change at the same values of the parameter, at $v_0 = \pm h$, leading to two double Hopf bifurcations.
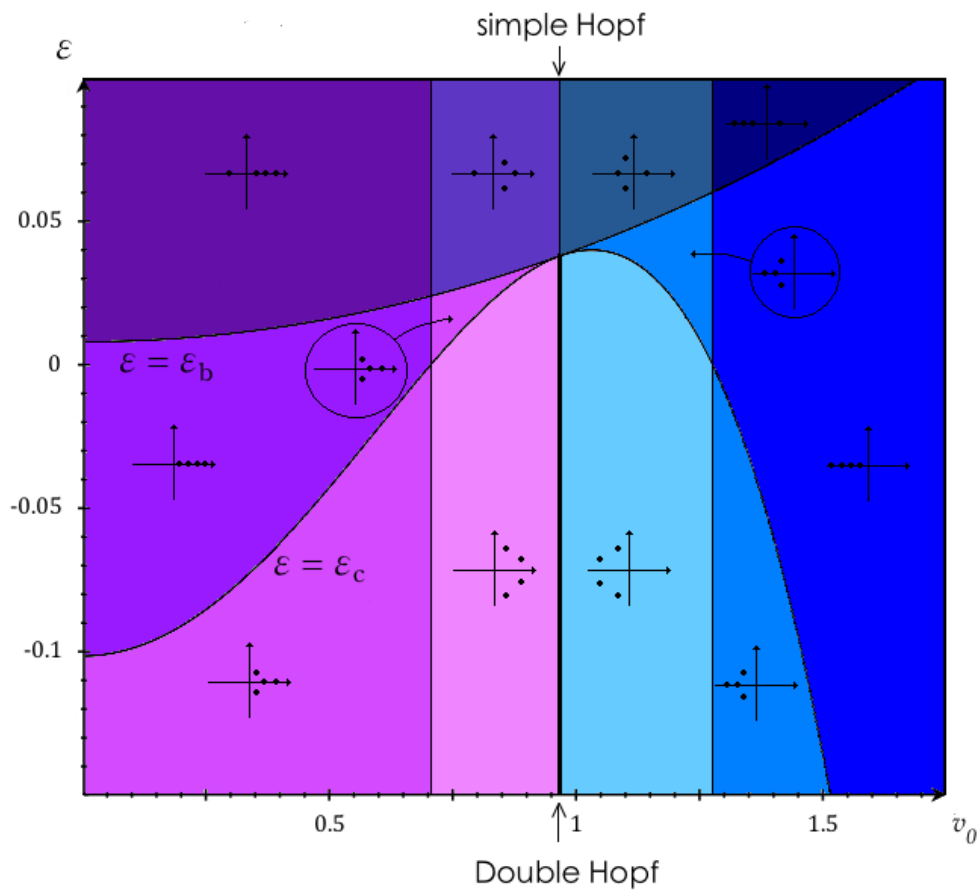

Figure 2.5 – Distribution of the eigenvalues of the Jacobian matrix at P_0 as a function of the coupling parameter ε and the coordinate v_0 of the equilibrium point.

In the case of the single oscillator, we recall that the real parts of the eigenvalues λ_1 and λ_2 were positive for $v_0 \in H$, and negative otherwise. This still

holds here for λ_1 and λ_2, but not quite for λ_3 and λ_4, since the discriminant Δ' depends not only on v_0, but also on the value of the coupling ε. In fact, when $\varepsilon > \varepsilon_c$, if $\sqrt{\Delta'} < |b\delta + v_0^2 - 1|$, then the eigenvalues λ_3 and λ_4 are of the same sign, which depends on whether or not v_0 is in the set H; otherwise, λ_3 and λ_4 have opposite signs.

An explicit function of v_0 can be found to delimit the region in the plane (v_0, ε) of the parameters where these scenarios occur, namely

$$
\begin{aligned}
& \Delta' < (b\delta + v_0^2 - 1)^2 \\
\Leftrightarrow & (b\delta + v_0^2 - 1)^2 - 4[\delta(1 - b(1 - v_0^2)) - 2\varepsilon] < (b\delta + v_0^2 - 1)^2 \\
\Leftrightarrow & \delta(1 - b(1 - v_0^2)) - 2\varepsilon > 0 \\
\Leftrightarrow & \varepsilon < \frac{\delta(1 - b(1 - v_0^2))}{2} =: \varepsilon_b .
\end{aligned}
\tag{2.19}
$$

This curve $\varepsilon = \varepsilon_b(v_0)$ provides the boundaries of the aforementioned regions. It is not too difficult to verify that $\varepsilon_c \leqslant \varepsilon_b$ for all values of v_0, and, consequently, this only affects the change of signs when λ_3 and λ_4 are real-valued. For parameter values on this curve, the eigenvalues are $\lambda_3 = \lambda_4 = 0$, which means that on these parameter curves P_0 is a branch point, giving birth to new branches of equilibrium points. Since $\varepsilon_b(v_0)$ is a quadratic polynomial that is positively oriented and has $v_0 = 0$ as vertical axis of symmetry, then, for a given ε, there can be zero, one, or two of these specific points on the branch of P_0. The minimum of ε_b, obtained when $v_0 = 0$) corresponds to the degenerate case where there is only one point with two zero eigenvalues, and is equal to $\delta(1 - b)/2 = 0.008$. This last result is consistent with what was observed with XPPAUT and stated in section 2.3.1.

The results of the calculations of this section are summarized in figure 2.5 in the plane of the parameters (v_0, ε) : we can observe the curves $\varepsilon = \varepsilon_c(v_0)$,

$\varepsilon = \varepsilon_b(v_0)$, the Hopf bifurcation line $v_0 = h$, and the lines $v_0 = \sqrt{u_1}$ and $v_0 = \sqrt{u_2}$ which define the positive interval where λ_1 and λ_2 are complex-valued. The interest for including the different distributions of the eigenvalues and the symmetry in v_0 explain the choice of the range of the parameters. Each zone has a color referring to a particular distribution of the eigenvalues on the complex plane, which is also illustrated on small diagrams. The blue regions correspond to the 'more' stable ones, with 3 or 4 eigenvalues with negative real part, whereas the violet regions yield parameter values for 'more' unstable states.

Notice that the curves $\varepsilon = \varepsilon_c(v_0)$ and $\varepsilon = \varepsilon_b(v_0)$ are tangent at $v_0 = \pm h$ and $\varepsilon = \delta(1 - b^2\delta)/2 \approx 0.038$. At this value, the still occuring Hopf bifurcation is no longer a double Hopf bifurcation. This can be interpreted as the death of one of the two coexisting cycles emerging form the double Hopf bifurcation of P_0. We can also note that as ε increases, the branch of the P_0 equilibrium point loses its stability.

2.3.3 Numerical Results

In order to determine the dynamics of the coupled system (2.12), we first apply a change of variables that exploits the particular rôle of the hyperspace defined by the relation $v_1 = v_2$. We thus introduce the variables

$$
\begin{cases}
x_1 = v_1 - v_2 \\
x_2 = v_1 + v_2 \\
y_1 = w_1 - w_2 \\
y_2 = w_1 + w_2,
\end{cases}
\tag{2.20}
$$

which transforms the original coupled system into the following :

$$\begin{cases} \dot{x}_1 = x_1 - x_1(x_1^2 + 3x_2^2)/12 - y_1 \\ \dot{x}_2 = x_2 - x_2(3x_1^2 + x_2^2)/12 - y_2 + 2is \\ \dot{y}_1 = x_1(\delta - 2\varepsilon) - b\delta y_1 \\ \dot{y}_2 = \delta(x_2 + 2a - by_2). \end{cases} \quad (2.21)$$

In this notation, it becomes clear that $x_1 = y_1 = 0 \Rightarrow \dot{x}_1 = \dot{y}_1 = 0$, which means that the plane

$$\mathcal{P} = \{(x_1, x_2, y_1, y_2) : x_1 = 0, y_1 = 0\},$$

is invariant for system (2.21). Moreover, all solutions on this plane satisfy a two-dimensional FitzHugh-Nagumo system which is independent of the coupling parameter ε :

$$\begin{cases} \dot{x}_2 = x_2 - \frac{1}{12}x_2^3 - y_2 + 2is \\ \dot{y}_2 = \delta(x_2 + 2a - by_2). \end{cases} \quad (2.22)$$

Therefore, the dynamic behavior described in Section 2.1 above also applies to this system, with only notational modifications. This means that the only asymptotically stable sets in this invariant plane are a single equilibrium point and a limit cycle. The dynamics on $\mathcal{P}$ are independent of ε, but the total stability is influenced by the other directions in the full 4-dimensional phase space. We can see this more clearly in the bifurcation diagrams displayed in figures 2.6, 2.10b and 2.14.

In these, as in all bifurcation diagrams presented in this section, the coordinates in phase space are those of equations (2.21) instead of the original coordinates of the coupled system (2.12). The diagrams present x_1, x_2, or both, as a function of the input parameter is. The selection of specific values of the coupling parameter is motivated by the desire to determine and illustrate the different dynamical behaviours. In all these illustrations, the choice of colors and symvols is consistent across all diagrams, and is described in table 2.I.

Line color	Type of solution
black	stable steady state (with a four dimensional stable manifold)
purple	unstable steady state (repelling in at least one direction)
blue	stable periodic solution (all non trivial Floquet multipliers inside the unit circle)
light blue	unstable periodic solution (repelling in at least one direction)
shades of green	unstable periodic solution arisen from a bifurcation on another periodic solution branch

(a) Line color code

Symbol	Type of bifurcation
triangle (▲)	Hopf bifurcation
diamond (♦)	double Hopf bifurcation
star (☆)	torus bifurcation
black point (•)	period doubling bifurcation
blue point (○)	new branch bifurcation on a periodic solution branch

(b) Special points code

Tableau 2.I – Code of colors and symbols, consistent across all bifurcation diagrams.

As a first glance into the possible bifurcations, we observe in figure 2.6 that the steady state and the periodic solution on the subset $x_1 = 0$ have the same stability as in figure 2.2. In figure 2.10b, on the corresponding (vertical) periodic solution branch displayed in figure 2.6, we see two bifurcations from which another cycle, represented by a dashed green line, takes birth. The distance between each of these bifurcations determines the interval of *is* for which the periodic solution is stable. Note that this new green cycle is not entirely contained on the plane. In fact, there are two cycles for the same projection, we will see it later with the help of another projection in figure 2.10a.

In figure 2.14, we can also see the influence of the other directions in the full phase space on the equilibrium point P_0, namely when the branch points go beyond the Hopf bifurcations, their stability is no longer delimited by the Hopf points, but rather by the branch points : as they move away, the interval of values of *is* for which P_0 is unstable increases. This is due to the opposite signs of two of the eigenvalues of P_0, as mentioned earlier.

To determine the criticality of each of these two Hopf bifurcations, we recall that the equilibrium point from which the associated limit cycles emerge lies on the invariant set $\mathcal{P}$. It is therefore sufficient to compute the real Jordan form of the system (2.22) which can be written as

$$\begin{cases} \dot{X} = RX - MY - \frac{R+b\delta}{M}\frac{c}{4}Y^2 - \frac{b\delta}{12M}Y^3 \\ \dot{Y} = MX + RY - \frac{c}{4}Y^2 - \frac{1}{12}Y^3, \end{cases} \tag{2.23}$$

where $R := -\frac{1}{2}(b\delta - 1 + \frac{c^2}{4})$ and $M = \sqrt{-(1 - \frac{c^2}{4} - b\delta)^2 + 4\delta(1 - b(1 - \frac{c^2}{4}))}/2$ are, respectively, the real and imaginary parts of the eigenvalues of the jacobian matrix of equations (2.22) at the Hopf bifurcations. As in Section 2.2 above, we define c as the x_2-coordinate of the equilibrium point of the system (2.22). This allows us to express *is* as a cubic polynomial in c, and, since this polynomial happens to be monotone, indifferently use c or *is* as the bifurcation parameter. Thus, we compute by the usual method the Lyapunov number at the Hopf bifurcations

$(c = \pm 2\sqrt{1 - b\delta})$ to be $\alpha \approx 2.47 > 0$, and conclude that both bifurcations are subcritical.

We are now in a position to systematically analyze system 2.21 by letting ε take successive values, and present bifurcation diagrams as a function of the parameter *is*.
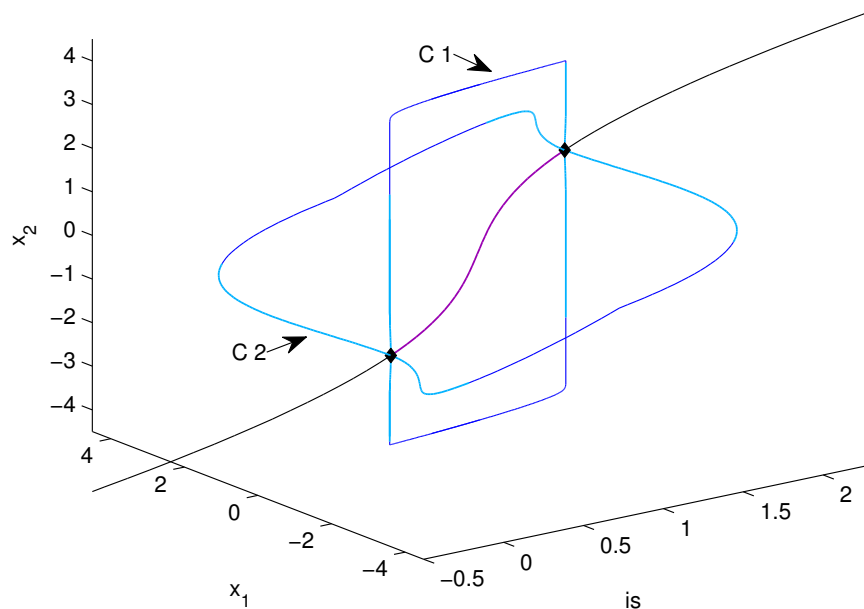

Figure 2.6 – Bifurcation diagram of equations (2.21) at the value $\varepsilon = -3$, (x_1, x_2) with respect to *is*. Here, we only show the unique steady state branch and the two periodic solutions arising from the double Hopf bifurcations C_1 and C_2. C_1 lies on the invariant plane $\mathcal{P}$. For the code of colors and symbols see table 2.I.

The first, and simplest case we consider, is shown in figure 2.6, illustrating the general behaviour observed for all negative values of ε. We see the unique equilibrium branch point corresponding to P_0 and the periodic solution in the invariant plane $\mathcal{P}$, the whole diagram being analogous, as mentioned before, to the one obtained for the single neuron, figure 2.2. In addition to this 'single'

diagram, we get a further limit cycle from the double Hopf bifurcations. The maximum and minimum of this cycle could have been expected to be symmetric with respect to the invariant plane, but as it happens, they are not. No other periodic solutions have been observed to emerge from the double Hopf bifurcations.

When the coupling parameter ε becomes positive, and remains close to zero, the complexity of the global dynamics increases, the bifurcations, and ensuing bifurcation diagrams, are slightly more involved at small values of the parameter. We try to now present their essential features. First, let us label the two limit cycles of figure 2.6 to help facilitate the following description. We name $\mathcal{C}_1$ the limit cycle lying on the invariant plane (the more square-shaped, vertically aligned one), and $\mathcal{C}_2$ the other cycle, arising from the double Hopf bifurcations. As mentioned before, $\mathcal{C}_1$ will keep its rectangular-like shape, while $\mathcal{C}_2$ will morph and split into two branches of periodic solutions intersecting with new steady states at heteroclinic bifurcations, before vanishing. At the value $\varepsilon = -0.05$, some changes have already taken place, the distance between the maximum and minimum values of $\mathcal{C}_2$ having increased. We observe this on figure 2.7, by comparing the bifurcation diagrams of the cycle in x_2 at the values $\varepsilon = -3$ (figure 2.7(a)) and $\varepsilon = -0.05$ (figure 2.7(b)). We also observe four bifurcation points on $\mathcal{C}_2$, represented as blue points, giving birth to new branches of periodic solutions. Let's recall that each of these bifurcations is represented by two points, one on the branch representing the maximum and the other one, the minimum of the limit cycle, we thus obtain eight points representing four bifurcations. Figure 2.7(c) is a glimpse at the complexity that begins to arise. Besides the periodic solution branch $\mathcal{C}_2$, we see branches arising from its bifurcation points. On the latter branches, we also find period doubling points, to which we shall return. Likewise, two period doubling bifurcations and two branch points will appear on $\mathcal{C}_1$, the bifurcations being situated as follows : a period doubling bifurcation near each of the Hopf bifurcation points, and the branch points at those values where changes of stability occur (figure 2.6). The branches appearing at these points exist for a small
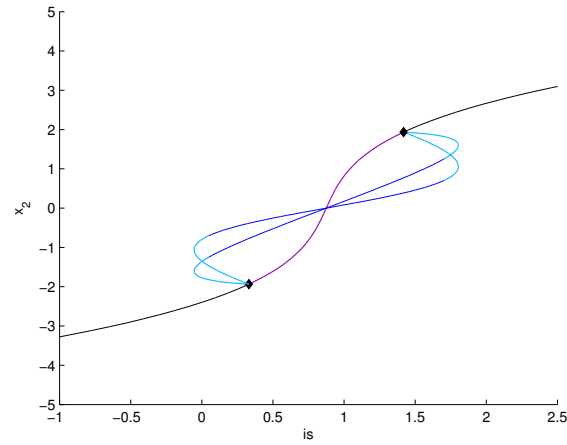
(a) Bifurcation diagram for $\varepsilon = -3$, x_2 vs is.
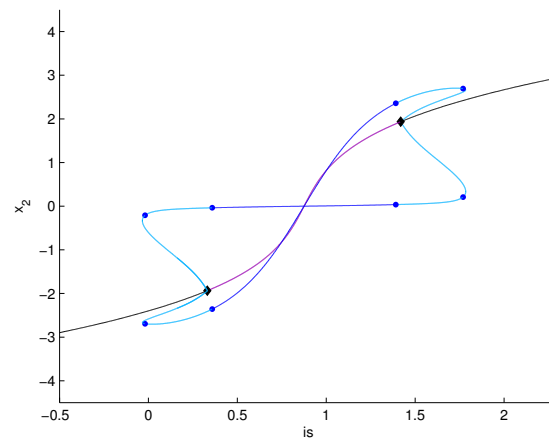
(b) Bifurcation diagram for $\varepsilon = -0.05$, x_2 vs is.
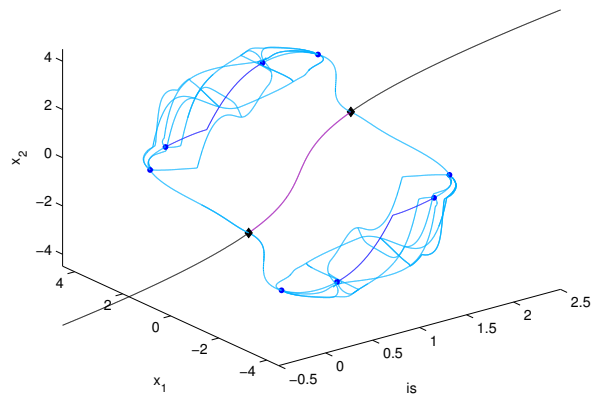
(c) Bifurcation diagram for $\varepsilon = -0.05$, (x_1, x_2) vs is.

Figure 2.7 – Bifurcation diagrams for $\varepsilon < 0$. On these three figures, we only show the steady state branch, cycle C_2, its bifurcation points and finally, in (c), the branches arising from them. For the code of colors and symbols see table 2.I.

interval, of length about $3 \cdot 10^{-3}$ in the parameter *is*, around the vertical portions of the C_1 branch, and do not lie on the invariant plane $\mathcal{P}$.

As ε is further increased, a new phase in the dynamical properties begins. We observe on figure 2.8(a), that the limit cycle C_1 is completely unstable, as seems to be the case for values of the coupling parameter as small as $\varepsilon = 10^{-6}$. Furthermore, the branch points seen previously disappear, but the period doubling bifurcations persist. The shape of the limit cycle C_2 has also undergone a slight modification, its unstable portions now staying closer to the values of the parameter *is* at which the double Hopf bifurcations occurred. We also display, in this figure, in green, a period doubling branch dying on C_1.

We can compare the branch arising from the period doubling points on C_1 and the C_2 branch, at the two values of the parameter ε displayed in figure 2.8. At $\varepsilon = 0.002$, figure 2.8 (a), the C_2 branch is unstable near the Hopf bifurcations form which it emerges, and stable on an intermediate interval of *is*. As for the branches arising from the period doubling points on C_1, in green, they die on the same C_1 branch. If we look now at the bifurcation diagram in figure 2.8 (b), where $\varepsilon = 0.006$, we notice a somewhat change of rôles between the branches of periodic solutions quoted above. Indeed, we can see that the C_2 branch is now separated in two branches each dying near the Hopf bifurcation it took birth in. As for the branches arising from the period doubling points, they now merge forming a unique branch, with two unstable portions near the bifurcations and stable in between. In addition, for $\varepsilon = 0.006$, we see the re-appearance of two branch points on C_1 bounding a stable portion of the branch. These new bifurcation points give birth to a periodic solution branch.

The bifurcations on the green period doubling branches and C_2 are omitted from figure 2.8. From these bifurcation curves emerge new branches which in turn give birth to other branches. The complexity of their organization becomes somewhat unyieldy : at the value $\varepsilon = 0.002$, for example, some of the branches born in C_2 appear to also have bifurcations with the period doubling branches, and vice versa.
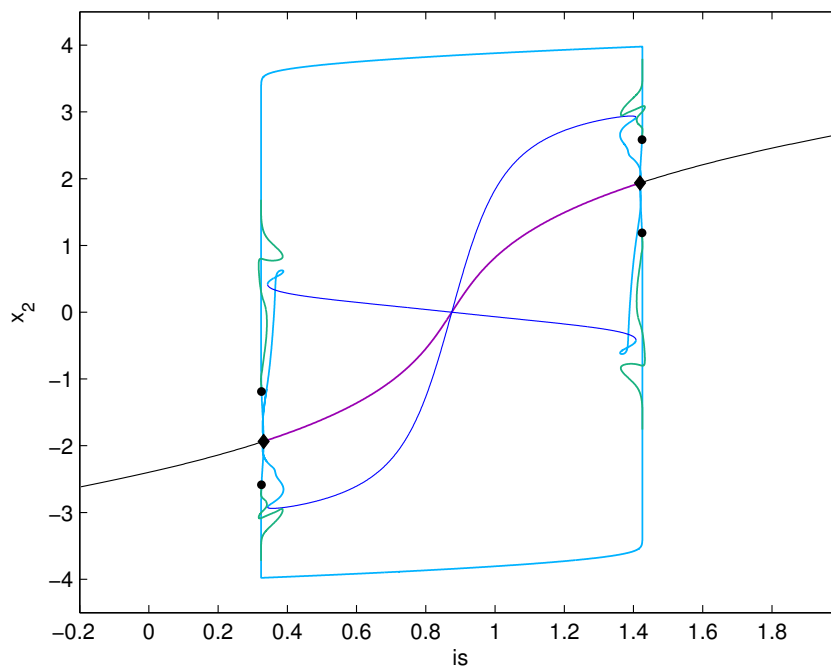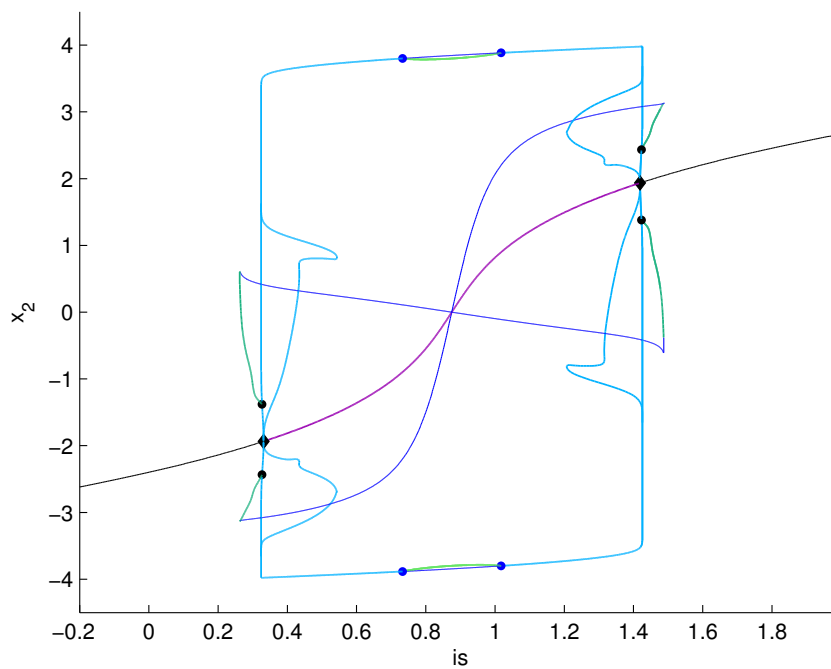
(a) Bifurcation diagram for $\varepsilon = 0.002$, x_2 vs *is*.

(b) Bifurcation diagram for $\varepsilon = 0.006$, x_2 vs *is*.

Figure 2.8 – Bifurcation diagrams for two representative values of small positive ε. Periodic solutions emerging from bifurcations on the period doubling branch and $\mathcal{C}_2$ are not shown. See table 2.I for colors and symbols.
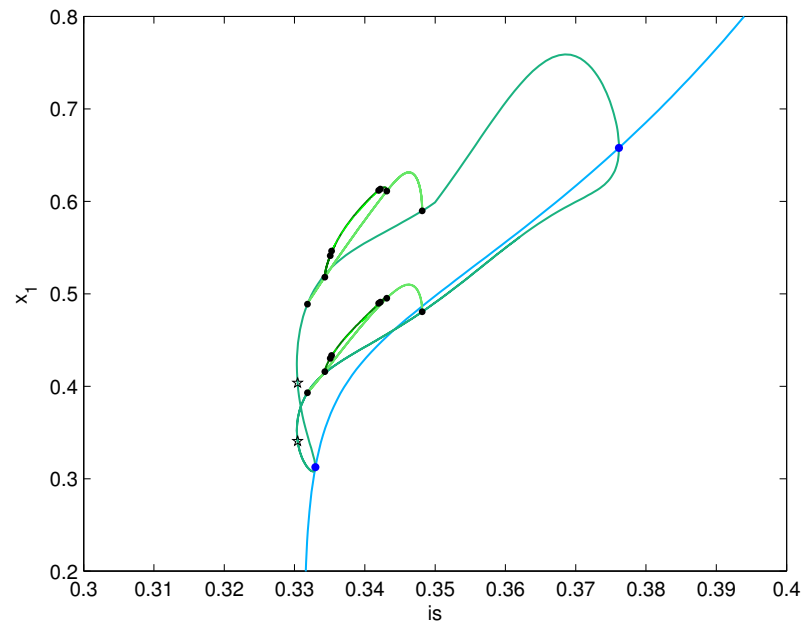
Figure 2.9 – Bifurcation diagram for ε = 0.0085, zooming on a series of period doubling solutions on the C_2 branch near the left Hopf bifurcation. We see only the maximum branches. See table 2.I for colors and symbols.

However, as ε is further increased, an interesting structure arises from some of the bifurcation branches initially emerging from C_2. Figure 2.9 is a zoom of the bifurcation diagram for ε = 0.0085 on the maximum branch of C_2, all solutions represented are unstable. At that value of ε, the shape of C_2 is the same as the one observed at ε = 0.006, namely the two branches born on the Hopf bifurcation branch merge with the invariant periodic solution C_1. Let's recall from the color convention blue points represent branch points, bifurcations on periodic solution branches giving birth to a new periodic solution branch ; and that black points stand for period doubling bifurcations. Here, we have a new type of bifurcation point, a torus bifurcation, represented by a star. The continuous light blue line indicates the maximum of the C_2 branch, and the different shades of green show the periodic solutions bifurcating from it. From the two branch points on C_2, we observe two new branches on each of which there are one to-

rus bifurcation and two period doubling bifurcations. On the period doubling branches that emerge, shown in lighter green, there are two period doubling bifurcations giving birth to a second period doubling branch, on which we will find again two period doubling bifurcations, and so forth. In the numerical simulations we performed at this value of the coupling parameter, we were able to observe up to three period doubling branches, and on the third one of these, we detected two more period doubling bifurcation points, which leads us to believe in the existence of a fourth period doubling branch. The distance between these successive period doubling branches and their parent branches becomes smaller at each level, and becomes of the same order as the step size of the continuation method, increasing the challenge in identifying them all. We conjecture nevertheless that there is an infinite number of period doubling branches.

As ε continues to increase, the two branches of steady solutions that have appeared at $\varepsilon = 0.008$ grow and have an increasing impact on the overall dynamical portrait, eventually simplifying the bifurcation scenarios. Thus, at $\varepsilon = 0.03$, we have a comprehensive bifurcation diagram illustrated in figures 2.10a and 2.10b : the two new branches of steady states are clearly visible, as they are symmetric with respect to the plane $\mathcal{P}$, and can be observed with different viewpoints on figures 2.10a and 2.10b, which are complementary projections from the three-dimensional space (x_1, x_2, is). As discussed at the end of section 2.3.2, since $\varepsilon < 0.038$, the Hopf bifurcations are still double ; and the changes of stability of P_0 occur at these points.

Focusing for the moment on the periodic solutions of P_0, we see in figure 2.10b that each of the double Hopf gives birth to two cycle branches corresponding to $\mathcal{C}_1$, in the invariant plane, and $\mathcal{C}_2$. Only here, $\mathcal{C}_2$ is separated in two parts which end in two homoclinic bifurcations on the new branches of equilibrium points. The branch from the left hand side Hopf bifurcation dies on the new equilibrium point situated above the plane $\mathcal{P}$ ($x_1 > 0$), and the other dies on the equilibrium point below it ($x_1 < 0$). The growing new branches of equilibrium
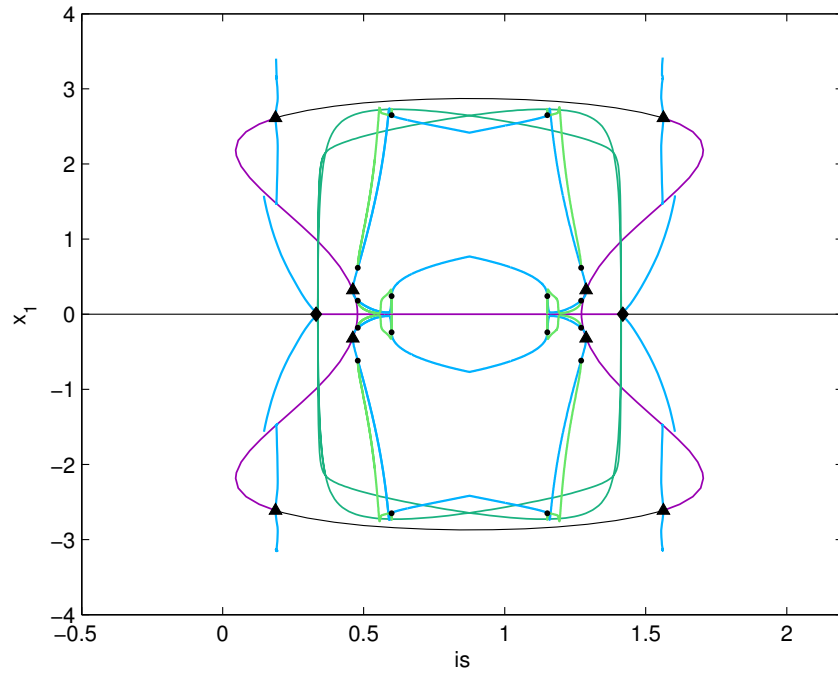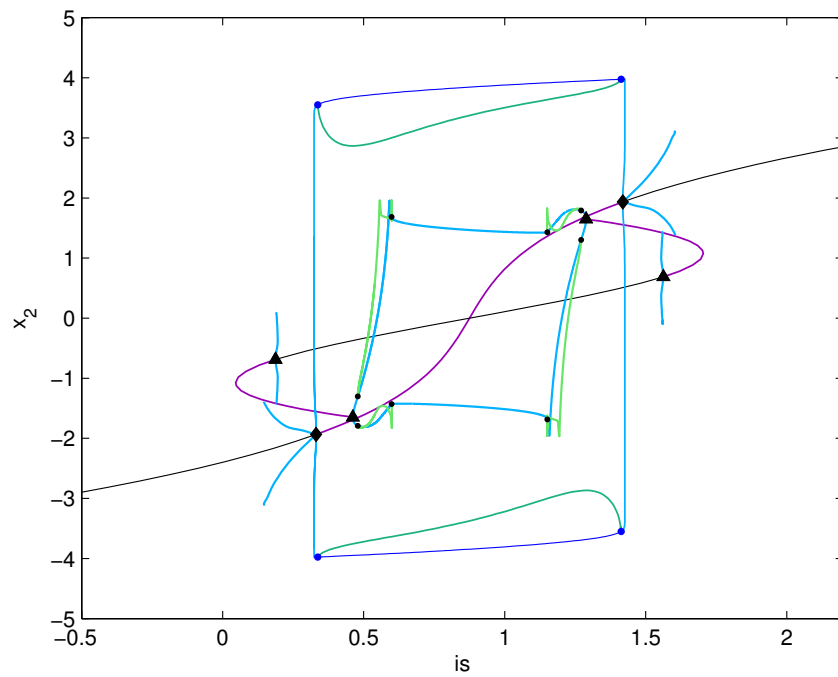
(a) x_1 vs *is*.

(b) x_2 vs *is*.

Figure 2.10 – Bifurcation diagrams for $\varepsilon = 0.03$. We can observe the complexity of the unstable periodic solutions. Note there are two periodic solutions in dark green, emerging from $\mathcal{C}_1$, rather than one (view from (b)), and that they do not lie on the invariant plane $\mathcal{P}$. See table 2.I for colors and symbols.

points eventually intercept C_2 into two homoclinic bifurcations. Even though it seems in figure 2.10a that there is a third (and even a fourth) branch of periodic solutions (in green) emerging from the Hopf bifurcation, figure 2.10b clearly shows that it is not the case. The green branches in this illustration are two periodic solution branches emerging and disappearing at the two branch points on the invariant cycle branch C_1. Similarly to what was observed for ε = 0.006 in figure 2.8(b), these branch points delimitate the stable part of the periodic solution branch, although the interval between them has grown, and will continue to do so up to a maximum reached at around ε = 0.04, before decreasing again and eventually vanishing. The invariant cycle C_1 then becomes completely unstable, as shown in figure 2.14. Although it may look otherwise, the two green branches are not symmetric with respect to $\mathcal{P}$. From figure 2.10b, the projection of the maxima branches are the same for both cycles, but a 3D view highlights the lack of symmetry. Equal caution must be used in interpreting the minima branches.

The new branches of equilibrium points each have four Hopf bifurcations. Because of the symmetry of the steady state solutions, we need only describe the bifurcations on one of the branches. Even though the planar symmetry will not be conserved for the periodic solutions, there will be a central symmetry with respect to $(0,0,0,\frac{2a}{b})$ and $is = \frac{a}{b}$, which makes the dynamic similar at either side of the plane : we focus on the branch below $\mathcal{P}$ (figure 2.10a).

A first pair of Hopf bifurcations is linked by a branch of unstable periodic solutions, as we see in both figures 2.10a and 2.10b : call this branch C_3. The minima branch seems to get close to the negative x_1 equilibrium point branch (figure 2.10a), but again, this is a distortion attributed to a projection. A similar illusion appears in the representation of the maxima, where although the branch seems to get near P_0 at two values of is, it actually gets close to the invariant plane at those two values, but close to the branch P_0 only for $is \approx 0.59$. On the C_3 branch, there are four period doubling points, linked pairwise by a period doubling branch : two different magnitude zooms on the right hand period
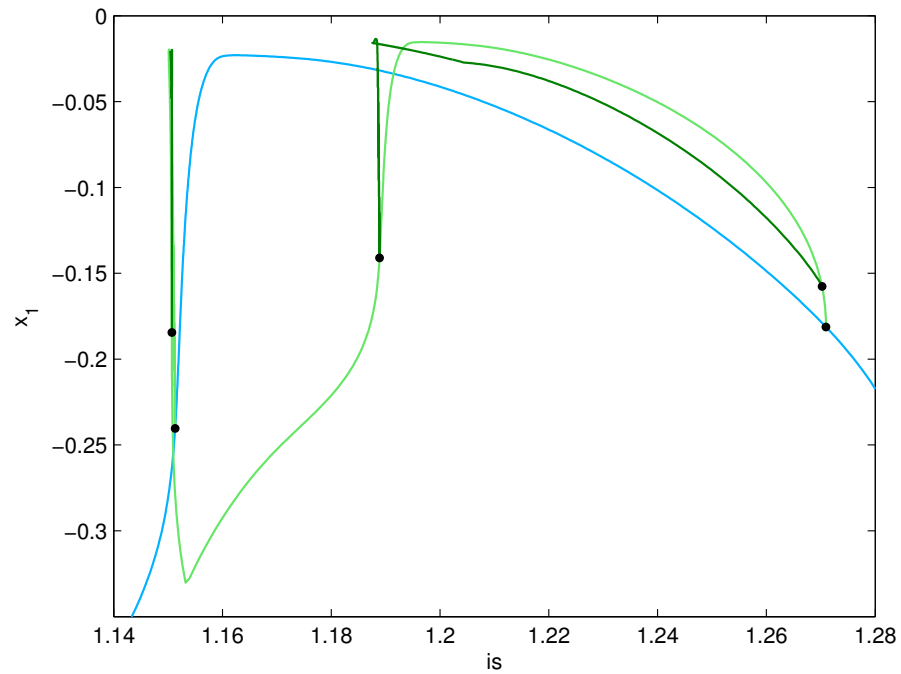
(a) Zoom on the C_3 and its period doubling branches. In light green we see a first PD branch, and in dark green, two other PD branches emerging from it.
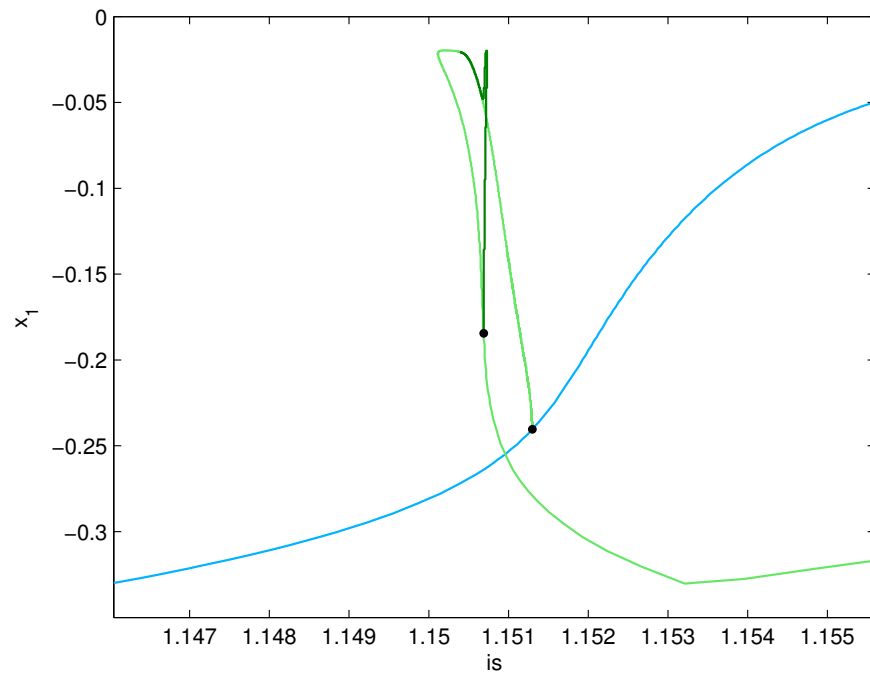
(b) Zoom on the left hand side (in (a)) period doubling bifurcation. We see that the dark green PD branch emerges from a single PD bifurcation. We suppose there is a second one but was not detected.

Figure 2.11 – Two different magnitude zooms of the bifurcation diagram for $\varepsilon = 0.03$, with x_1 vs is. See table 2.I for colors and symbols.

doubling branch, in light green, are shown in figure 2.11 ; here, C_3 is in light blue, as it is unstable. In figure 2.11(a), we see that from this branch two new period doubling branches, also unstable and shown in darker green, arise. Three period doubling bifurcation points were detected by the continuation, giving birth to the new period doubling branches. On the left new period doubling branch in lighter green (figure 2.11(a)), only one of the extremities is a period doubling bifurcation. Figure 2.11(b) displays this particular branch in more details, and it seems to asymptotically approach the original period doubling branch. Nevertheless, when we look at the period of the branch as it gets closer to the original branch, we see that it is still double. The way this branch ends is yet to be understood.

Returning to figures 2.10a and 2.10b, we can further describe the bifurcations on the new branches of equilibrium points. Aside the two Hopf bifurcations linked by a cycle branch, there are two other simple Hopf bifurcations at the endpoints of the new steady state's interval of stability. This second pair of bifurcations gives birth to two unstable cycles that end in a homoclinic bifurcation on the unstable portion of the equilibrium branch. The dynamics observed near those bifurcations have a particularly elegant geometric representation, shown in figure 2.12.

Indeed, we display the phase portrait of the dynamical system at $is \approx 0.1875$, in the (x_1, x_2)-plane, i.e. near the heteroclinic bifurcation of the unstable cycle arising from the left hand stability-delimiting Hopf bifurcation on the negative $(x_1 < 0)$ equilibrium branch. As predicted by the numerical continuation, there are a stable equilibrium point, P_0, with $x_1 = 0$, two stable steady states symmetric with respect to $x_1 = 0$, and two unstable steady states, symmetric, as well, with respect to this same hyperplane. Each of the latter equilibrium solutions has a heteroclinic orbit, whose respective invariant unstable manifolds look like a moth : the manifold corresponding to the negative $(x_1 < 0)$ unstable equilibrium point is shown in blue, whereas the manifold corresponding to the positive $(x_1 > 0)$
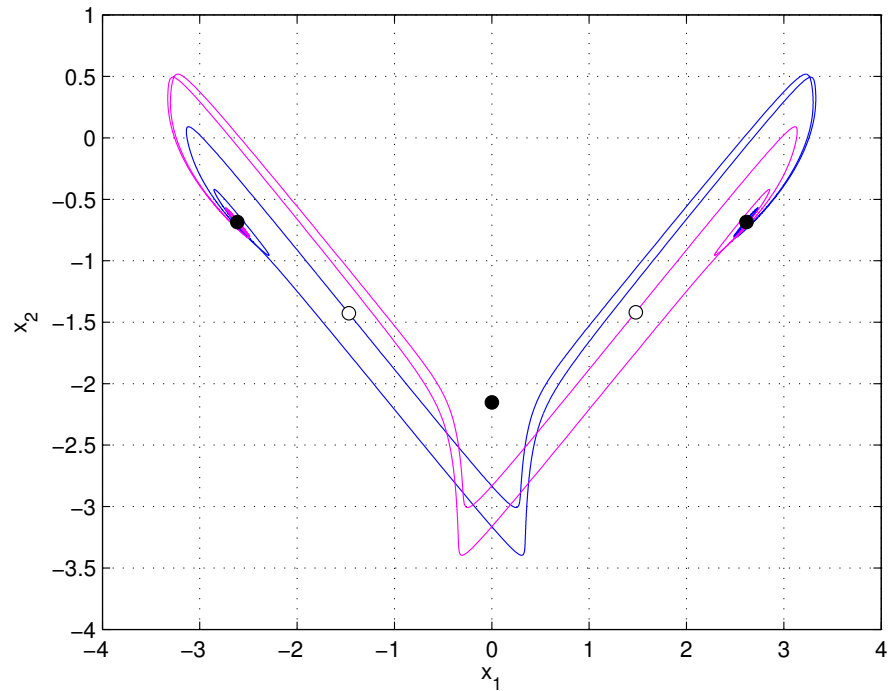
Figure 2.12 – Phase portrait of invariant unstable manifolds at heteroclinic bifurcation ($\varepsilon = 0.03$ and $is \approx 0.1875$). In magenta, we see the unstable manifold of the positive ($x_1 > 0$) unstable steady state, the trajectory of which tends to the negative ($x_1 < 0$) stable steady state. The opposite observation can be made about the negative ($x_1 < 0$) unstable steady state manifold in blue.

unstable equilibrium is displayed in magenta. The symmetry between them is clear. A curious observation is that in each of the two unstable directions, the trajectory on these manifolds will tend to the stable steady state at the other side of the plane $\mathcal{P}$. That is, if we induce a negative perturbation of the negative unstable equilibrium, on the manifold, that trajectory will turn around the negative stable equilibrium before converging to the positive stable equilibrium. If the perturbation is positive (in the opposite direction), the trajectory will directly go to the other side of $\mathcal{P}$ towards the positive stable equilibrium. Similarly, the solutions on the positive equilibrium unstable manifold will converge to the negative stable steady state.

The value of the coupling parameter $\varepsilon = 0.038$ is a significant one, since it is where the Hopf bifurcations of P_0 become simple, and merge with the pitchfork bifurcations while the periodic solution C_2 vanishes. It corresponds to the value of ε where the ε_b and ε_c curves intersect with the Hopf bifurcation line in figure 2.5. This value is also critical for the Hopf bifurcations on the new branches of equilibrium points, the ones that gave birth to a branch C_3 of periodic solutions : they move towards the Hopf bifurcations of P_0, and eventually disappear. Obviously, the apparent simplification of the global dynamics reached at $\varepsilon = 0.03$ is replaced by a number of periodic solutions emerging from the C_1 branch. These appear in all likelihood from the interaction between the different Hopf and pitchfork bifurcations giving rise to secondary bifurcations. In addition, the branch points that limited at previous values the stable portion of the branch C_1 have become period doubling bifurcations. At $\varepsilon = 0.04$, as already mentioned, they go back to being branch points and the distance between them reaches its maximum, decreasing as ε is further increased until it becomes null when $\varepsilon = 0.05$.

One feature worth highlighting occurs at $\varepsilon = 0.06$ and is illustrated in figure 2.13. At this value of the coupling parameter, we have the two invariant stationary solutions P_0 and C_1, now completely unstable and devoid of further bifurcation points, the two new branches of equilibrium points, as well as the cycles from the stability-delimiting Hopf bifurcations (two on each new branch of steady states). Figure 2.13 is a zoom on one of these cycles, and shows that the bifurcation diagram in the neighbourhood of the stability changes of the new branches of equilibria is different from all previous diagrams : a new Hopf bifurcation has appeared on the unstable portion of the branch, on the other side of the limit point, point marking a change of directions of a branch in all coordinates. The cycle no longer ends in a heteroclinic bifurcation, but rather on the new Hopf bifurcation, as follows from the evolution of the eigenvalues of the equilibrium point. In this case, a pair of complex eigenvalues goes back (first Hopf bifurcation) and forth (second Hopf bifurcation) through the imaginary axis, while a positive real eigenvalue becomes negative at the limit point. This
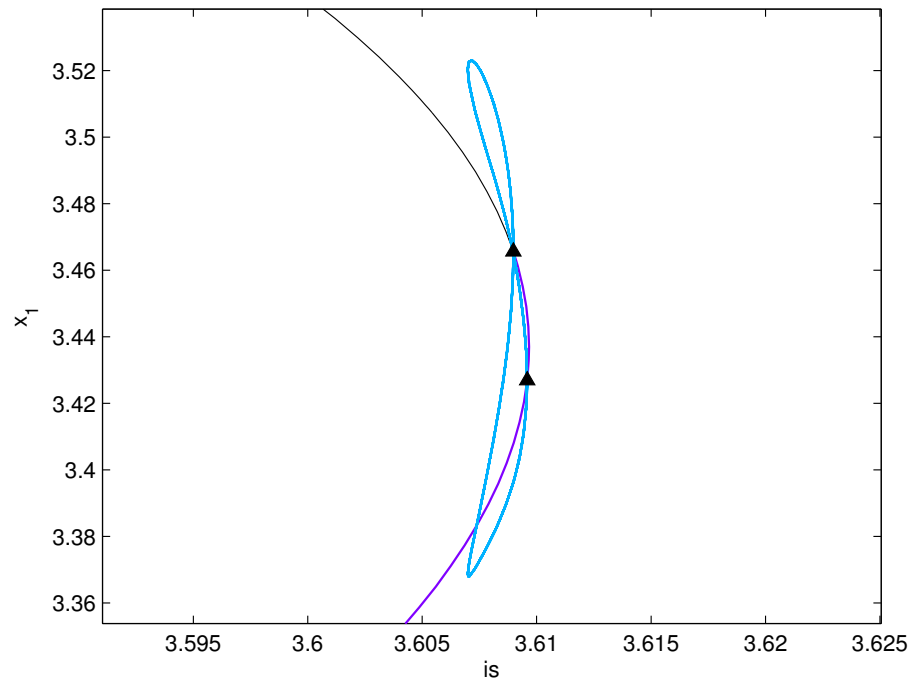
Figure 2.13 – Bifurcation diagram for $\varepsilon = 0.06$, x_1 vs is. Zoom on the positive ($x_1 > 0$) steady state branch, on the right hand Hopf bifurcation delimiting the stable and unstable portions of the branch. We see a new single Hopf bifurcation on the unstable portion, and an unstable cycle linking the two bifurcations. See table 2.I for colors and symbols.

motion of the real parts of the eigenvalues will have ceased at $\varepsilon = 0.07$, when only the real positive eigenvalue will persist in going through the imaginary axis, and the change of stability will occur at the limit point.

For the last value we consider, figure 2.14 represents the three-dimensional bifurcation diagram of system (2.21) at $\varepsilon = 0.1$. Since this system is a linear transformation of equations (2.12), they display identical dynamical behaviors for the same values of the parameters is and ε. The dynamical behavior portrayed here is therefore also the one occuring for all values of $\varepsilon > \delta/2 = 0.04$. Indeed, as discussed in section 3.2.2, this is the initial value of the parameter at which the interval of is where the eigenvalues $\lambda_{3,4}$ are complex conjugate no longer exists. All bifurcations observed up to this value have now vanished except for the
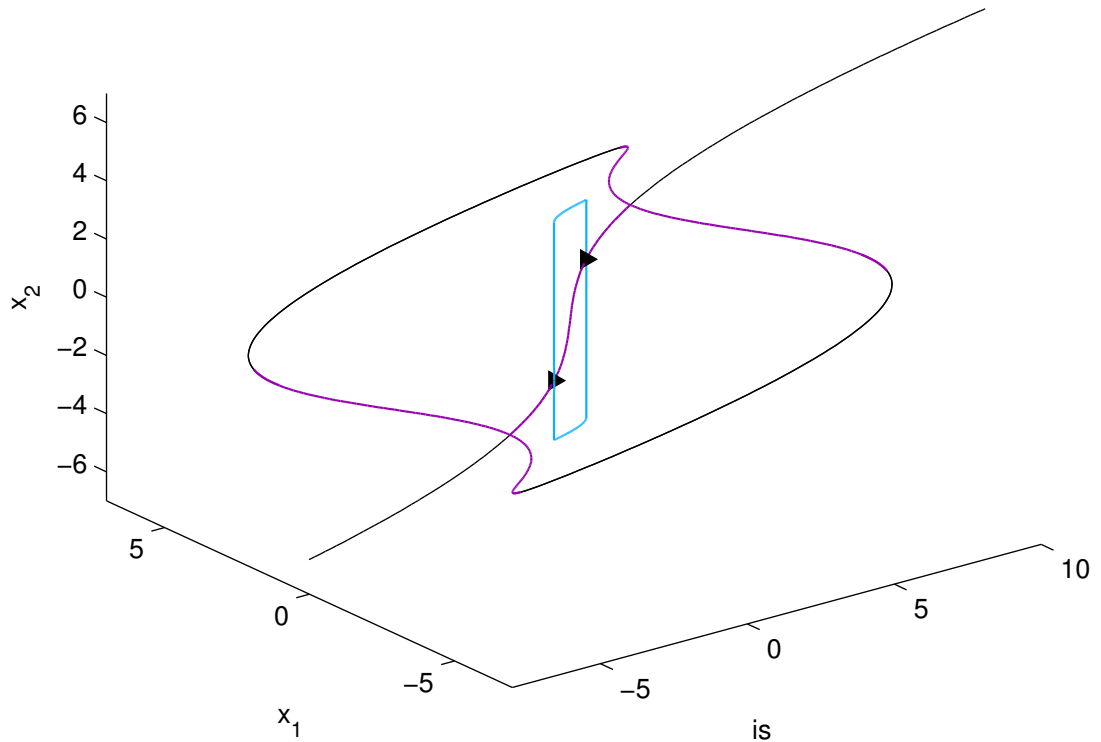
Figure 2.14 – Bifurcation Diagram for $\varepsilon = 0.1$, (x_1, x_2) vs is. Only the steady state solutions and the now unstable $\mathcal{C}_1$ branch persist. See table 2.I for colors and symbols.

branch points giving rise to the new branches of equilibrium steady states and their leap points. The asymptotic set has settled to a simple structure : there is a unique unstable periodic solution, and as ε further increases, the branch points on P_0 grow apart and for an increasing interval in is, there are two symmetrical and stable steady states, and an unstable one. Essentially, all solutions converge to one of the two complementary equilibrium points.

2.4 Discussion

We have presented, through a combination of analytical and numerical methods, the bifurcation structure of a system of two coupled FitzHugh-Nagumo oscillators. To rely on simulations alone would have been insufficient to determine the range of possible dynamics, and would not have allowed the level of comprehension of the system the diversity of approaches we employed permits.

The coupling we introduced was motivated initially by an attempt to model the neural activity influencing the sinus node with a network of Hindmarsh-Rose oscillators [2]. One of the questions that arose from the results concerned the determination of the real source of the dynamical particularities observed, namely to assess whether it was due to the spiking-bursting behavior of the model (Hindmarsh-Rose), or to the symmetric coupling on the slow variables of the oscillators. Using a simplified model of neurons, namely FitzHugh-Nagumo oscillators, and preserving the nature of the coupling, we were able to conclude that the particularities were due, in fact, to the coupling, and the relative simplicity allowed us to determine the dynamical behavior in some details.

We have obtained that there is a stationary solution P_0, where both oscillators are identical to the equilibrium point of a single oscillator, and that this solution is independent of the coupling parameter ε. This result is more generally true for any system of two oscillators with a unique stationary solution. Two other equilibrium branches appear at $\varepsilon = 0.008$, and for increasing coupling values, the family branch P_0 loses its stability as the two other branches and their stable interval expand, see Figure 2.14. Those last branches are equivalent since one branch corresponds to a swap of rôles between the oscillators with respect to the other branch. Therefore, as the coupling increases further, the oscillators will converge to a non-identical state for a wider interval of the input current parameter is.

However, the most remarkable feature displayed in this system is that from a pair of oscillators as simple as FitzHugh-Nagumo, we managed to generate,

with a symmetric coupling, dynamics of such complexity. With the coupling term ε near zero, we find an interesting diversity of interacting invariant sets, such as ordinary periodic solutions, period doubling solutions and tori. It is likely that the peculiar coupling term is responsible for this dynamical complexity. In future work, it would be interesting to construct the three-dimensional unstable invariant surfaces in order to observe a stable torus, the existence of which is strongly suggested by values of the parameters *is* and ε for which the periodic solution that generates the torus has two stable Liapunov numbers and an unstable one.

This study provides further evidence of the superior potential for rich behavior in FitzHugh-Nagumo systems, as illustrated by Campbell and Waite [3], in contrast with the much studied, in various forms of coupling, Van der Pol, oscillators which exhibit milder behavior. However, it also brings out an important question about the level of complexity we seek, and we need, in neuron models to capture a set of particular dynamics. It is likely that a coupling such as the one studied in this paper, but applied to a detailed and more biologically realistic neuron model, such as Hindmarsh-Rose or Hodgkin-Huxley, would render an analytico-numerical study such as the one presented here, difficult if not impossible. To what extent, in this context, can we assess all possible behaviors in a system, and the rôle of the regulating parameters ? A series of numerical simulations, however systematic, are likely to identify but a fraction of the possible behaviors.

CHAPITRE 3

CONCLUSION

L'objectif principal des recherches effectuées dans le cadre de ce mémoire était la compréhension globale de la dynamique du système de deux oscillateurs FHN couplés sur la variable lente. On a donc privilégié une analyse somme toute conventionnelle, détermination des valeurs propres d'un point d'équilibre, et la continuation numérique aux simulations par méthodes d'intégration.

Les résultats dans la première partie de l'article, sont le fruit d'une étude analytique des valeurs propres de la solution sationnaire unique d'un oscillateur FHN simple, en fonction du paramètre I, représentant le courant appliqué. Ayant détecté l'existence de bifurcations de Hopf, on a procédé au calcul des exposants de Lyapunov pour confirmer le diagramme de bifurcation obtenu avec le logiciel XPPAUT.

Dans la deuxième partie, concernant cette fois les deux oscillateurs couplés, on a pu obtenir grâce à la symétrie du couplage, un diagramme de la distribution des valeurs propres dans le plan complexe pour un des points d'équilibre, en fonction du paramètre I et du paramètre de couplage ε. Il aurait été intéressant de pouvoir en faire autant avec les deux autres branches de solutions stationnaires, mais l'impossibilité d'obtenir une expression analytique de ces dernières, de même que les limites de temps intrinsèques à un travail de maitrise, a limité nos efforts dans cette direction.

Un calcul des exposants de Lyapunov des bifurcations de Hopf, cette fois-ci dans le plan invariant $\mathcal{P} = \{x_1 = 0, y_1 = 0\}$, a pu confirmer de nouveau le caractère sous-critique de celles-ci.

Enfin, une série de diagrammes de bifurcation effectués pour un intervalle assez large de valeurs du paramètre de couplage ε a permis l'identification de certains états dynamiques considérés intéressants, soit par la particularités des solutions, soit par la place clé qu'ils ont au sein d'une évolution par rapport au

paramètre de couplage. Une grande complexité émerge autour de $\varepsilon = 0$. Sur les deux cycles principaux (liés aux doubles bifurcations de Hopf), on voit naître de nouvelles branches de solutions périodiques venant de points de bifurcations, et sur ces nouvelles branches d'autres branches se créent en des bifurcations de doublement de période. En $\varepsilon = 0.0085$, on arrive même à une succession de branches de doublement de période , que les limites computationnelles nous ont empêché de décrire complètement. À $\varepsilon = 0.03$, nous avons pu construire avec XPPAUT les trajectoires invariantes liant deux des points fixes, une bifurcation hétéroclinique ($is \approx 0.1875$) donnant naissance à un objet en forme de mite.

La dynamique générée par le couplage considéré dans ce mémoire est riche et plusieurs questions restent en suspens, notamment, au sujet des points de bifurcation donnant naissance à un tore. Le programme de continuation numérique XPPAUT se base sur des critères analytiques pour déterminer l'existence de points de bifurcation spécifiques. Dans notre cas, nous n'avons pas pu observer par simulations les tores en question : ceci peut être dû à leur instabilité, totale ou partielle. La distribution des valeurs propres associées à ces points de bifurcation nous porte à croire qu'il serait possible de construire une surface invariante instable sur laquelle on pourrait observer un tore stable.

Il a été fascinant de constater dans ce travail la richesse qui pouvait être issue d'un couplage symétrique sur deux oscillateurs simples comme ceux de FitzHugh-Nagumo. Ceci nous mène naturellement à la question, existentielle, suivante : la complexité persisterait-elle avec le modèle classique de van der Pol, très étudié dans la littérature, mais n'ayant jamais engendré, sur la seule base du couplage, une dynamique aussi élaborée ? De même, à quoi pouvons-nous nous attendre dans le cas de plusieurs oscillateurs couplés de telle façon ? On peut aussi s'interroger sur le type de réseaux d'oscillateurs pour lesquels ce couplage est représentatif : correspond-il à la communication inter-cellulaire présente dans le noeud sinusal ?

À travers le cheminement qui a mené à ce mémoire, un questionnement, au-delà de l'objectif de l'article, a émergé.

Le but de cette recherche était de capter une dynamique globale, mais celle-ci s'est avérée plus riche que prévue. Le modèle de FitzHugh-Nagumo n'étant décrit que par deux équations et ne pouvant reproduire des phénomènes tels que le *bursting*, ne laissait pas prévoir de tels résultats. Et il est encore ardu, malgré le travail effectué, de saisir l'ensemble des informations dans les diagrammes de bifurcation. L'évolution en est difficile à apprivoiser, même après en avoir été imprégnée pendant des mois. On peut alors essayer d'imaginer ce qu'il en serait d'appliquer ce même couplage à un réseau de neurones représenté par un modèle détaillé de plusieurs équations reproduisant des phénomènes exotiques. Dans quel sens et, surtout, dans quelle mesure, pouvons-nous prétendre à la compréhension de la dynamique globale d'un tel système ?

Les avancées dans les performances technologiques nous permettent de faire de plus en plus de calculs en moins de temps, et la perspective de pouvoir faire des modèles de plus en plus détaillés devient alléchante. La difficulté fondemantale demeure néanmoins la capacité de saisir la dynamique globale de systèmes couplés d'oscillateurs plus complexes : le modèle de Hindmarsh-Rose est-il à notre portée ? et pour des réseaux ? Qu'est-ce qu'on cherche exactement, et quel type de compréhension pouvons-nous en tirer ? Les résultats présentés ici suggèrent minimalement un septicisme de bon aloi sur l'utilisation débridée de la puissance computationnelle qui, malgré une reproduction informatique mimétique du système biologique, ne peut se substituer à une connaissance profonde des mécanismes sous-jacents.

BIBLIOGRAPHIE

[1] J. Bélair et P. Holmes. On Linearly Coupled Relaxation Oscillations. *Quaterly of Applied Mathematics*, pages 193–219, juillet 1984.

[2] P.L. Buono, A. Vinet et J. Bélair. Bifurcation Analysis of Symmetrically Coupled Fast/Slow Systems. Dans *International Conference on Applications in Nonlinear Dynamics (ICAND 2010) AIP Conf. Proc. 1339*, pages 222–235, 2011.

[3] S. A. Campbell et M. Waite. Multistability in Coupled FitzHugh-Nagumo Oscillators. *Nonlinear Analysis*, 47:1093–1104, 2001.

[4] Bard Ermentrout. XPP/AUT Homepage, 2012. URL http://www.math.pitt.edu/~bard/xpp/xpp.html.

[5] R. A. Fisher. The Wave of Advance of Advantageous Genes. *Ann. Eugen.*, 7:355–369, 1937.

[6] R. FitzHugh. Thresholds and Plateaus in the Hodgkin-Huxley Nerve Equations. *J. Gen. Physiol*, 43:867Đ896, 1960.

[7] W. Gerstner et R. Naud. How Good Are Neuron Models ? *Science*, 326: 379–380, 2009.

[8] J. Guckenheimer et P. Holmes. *Nonlinear Oscillations, Dynamical Systems, and Bifurcations of Vector Fields*, volume 42 de *Applied Mathematical Sciences*. Springer, 1983.

[9] A. V. M. Herz, T. Gollisch, C. K. Machens et D. Jaeger. Modeling Single-Neuron Dynamics and Computations : A Balance of Detail and Abstraction. *Science*, 314:80–85, 2006.

[10] J.L. Hindmarsh et R.M. Rose. A Model of Neuronal Bursting Using Three Coupled First Order Differential Equations. *Proc. R. Soc. Lond. B*, 221:87–102, 1984.

[11] A.L. Hodgkin et A.F. Huxley. A Quantitative Description of Membrane Current and its Application to Conduction and Excitation in Nerve. *J. Physio.*, 117:500–544, 1952.

[12] E. M. Izhikevich et R. FitzHugh. FitzHugh-Nagumo Model. *Scholarpedia*, 1 (9):1349, 2006.

[13] G. S. Medvedev. Synchronization of Coupled Limit Cycles. *J. Nonlinear Sc.*, 21:441–464, 2011.

[14] C. Meunier et I. Segev. Playing the Devil's Advocate : Is the Hodgkin-Huxley Model Useful ? *TRENDS in Neuroscience*, 25(11):558–563, 2002.

[15] J. G. Milton. *Dynamics of Small Neural Populations*. CRM Monograph Series, AMS, 1996.

[16] J. Nagumo, S. Arimoto et S. Yoshizawa. An Active Pulse Transmission Line Simulating Nerve Axon. *Proc. IRE*, 50:2061–2070, 1962.

[17] T. Nordhaus. *Echo-Cycles In Coupled FitzHugh Nagumo Equations*. Thèse de doctorat, University of Utah, 1988.

[18] I. Pastor-Díaz et A. Lopez-Fraguas. Dynamics of Two Coupled van der Pol Oscillators. *Physical Review E*, 52(2):1480–1489, 1995.

[19] C. Roşoreanu, A. Georgescu et N. Giurgiteanu. *The FitzHugh-Nagumo Model*. Kluwer Academic Publishers, 2000.

[20] A. I. Selverston et J. Ayers. Oscillations and Oscillatory Behavior in Small Neural Circuits. *Biological Cybernetics*, 95:537–554, 2006.

[21] A. K. Sen et R. H. Rand. Dynamics of Two Time-Delay Coupled Relaxation Oscillators of the van der Pol Type. Dans *Dynamics, Acoustics and Simulations*, 2000.

[22] A. K. Sen et R. H. Rand. A Numerical Investigation of the Dynamics of a System of Two Time-delay Coupled Relaxation Oscillators. *Communications on pure and applied analysis*, 2(4):567–577, 2003.

[23] D. Storti. Bifurcations Which Destroy the Out-of-phase Mode in a Pair of Linearly Coupled Relaxation Oscillators. *Int. J. Non-Linear Mechanics*, 22(5): 387–390, 1987.

[24] D. Storti et R. H. Rand. Dynamics of Two Strongly Coupled van der Pol Oscillators. *Int. J. Non-Linear Mechanics*, 17(3):143–152, 1982.

[25] D. Storti et R. H. Rand. A Simplified Model of Coupled Relaxation Oscillators. *Int. J. Non-Linear Mechanics*, 22(4):283–289, 1987.

[26] D.W. Storti et R. H. Rand. Dynamics of Two Strongly Coupled van der Pol Oscillators. *SIAM. J. Appl. Math.*, 46:56–67, 1986.

[27] B. van der Pol et M. J. van der Mark. Le battement du coeur considéré comme oscillation de relaxation et un modèle électrique du coeur. Dans *Le battement du coeur*, volume 7, pages 365–392, 1928.

[28] A. Vinet. Communication personnelle (2010).

[29] V. Volterra. *Leçons sur la théorie mathématique de la lutte pour la vie*. Éditions Jacques Gabay, 1931.

[30] A. Winfree. *The Geometry of Biological Time*. Springer, 1980.